AUTOIMMUNITY

UNC93B1 variants underlie TLR7-dependent autoimmunity

**Christine Wolf[1], Ee Lyn Lim[2], Mohammad Mokhtari[3], Barbara Kind[1], Alexandru Odainic[4,5], Eusebia Lara-Villacanas[6], Sarah Koss[1], Simon Mages[3], Katharina Menzel[1], Kerstin Engel[1], Gregor Dückers[7], Benedikt Bernbeck[6], Dominik T. Schneider[6], Kathrin Siepermann[7], Tim Niehues[7], Carl Christoph Goetzke[8,9,10], Pawel Durek[9], Kirsten Minden[8,9], Thomas Dörner[9,11], Anna Stittrich[12], Franziska Szelinski[9,11], Gabriela Maria Guerra[9], Mona Massoud[9], Markus Bieringer[13], Carina C. de Oliveira Mann[14], Eduardo Beltrán[15], Tilmann Kallinich[8,9,10], Mir-Farzin Mashreghi[9], Susanne V. Schmidt[4], Eicke Latz[4,16], Johanna Klughammer[3], Olivia Majer[2], Min Ae Lee-Kirsch[1,17]*

UNC93B1 is critical for trafficking and function of nucleic acid–sensing Toll-like receptors (TLRs) TLR3, TLR7, TLR8, and TLR9, which are essential for antiviral immunity. Overactive TLR7 signaling induced by recognition of self–nucleic acids has been implicated in systemic lupus erythematosus (SLE). Here, we report UNC93B1 variants (E92G and R336L) in four patients with early-onset SLE. Patient cells or mouse macrophages carrying the UNC93B1 variants produced high amounts of TNF-α and IL-6 and upon stimulation with TLR7/TLR8 agonist, but not with TLR3 or TLR9 agonists. E92G causes UNC93B1 protein instability and reduced interaction with TLR7, leading to selective TLR7 hyperactivation with constitutive type I IFN signaling. Thus, UNC93B1 regulates TLR subtype–specific mechanisms of ligand recognition. Our findings establish a pivotal role for UNC93B1 in TLR7-dependent autoimmunity and highlight the therapeutic potential of targeting TLR7 in SLE.

INTRODUCTION

Endosomal Toll-like receptors (TLRs) play a fundamental role in detecting pathogen-derived nucleic acids. Single-stranded RNA (ssRNA) is recognized by TLR7 and TLR8, double-stranded RNA by TLR3, and single-stranded DNA by TLR9 (*1*, *2*). TLRs consist of a single-transmembrane α helix with a luminal ectodomain containing a leucine-rich repeat (LRR-CT motif) and a cytoplasmic Toll/interleukin-1 (IL-1) receptor (TIR) domain (*3*). Upon ligand recognition through the LRR-CT motif, the TIR domains of the TLR homodimer assemble to form signaling complexes. Activation of TLR7, TLR8, and TLR9 initiates recruitment of the adaptor protein myeloid differentiation primary–response protein 88 (MyD88), whereas engagement of TLR3 induces recruitment of TIR domain–containing adaptor protein (TRIF)–inducing interferon-β (IFN-β) (*1*, *2*). Both pathways lead to activation of IFN-regulatory factor 7 (IRF7), IRF3, and nuclear factor κB (NF-κB), resulting in induction of type I IFN and proinflammatory cytokines that mobilize host immune responses (*1*, *2*).

The multipass transmembrane chaperone UNC93 homolog B1 (UNC93B1) is required for the trafficking of TLRs from the endoplasmic reticulum to the endosome and acts as a scaffold for proper configuration of the TLR dimer within the endosomal membrane, which is critical for TLR signaling (*4*–*7*). The essential role of UNC93B1 for nucleic acid–sensing TLR function was unraveled by studying 3d mice, which harbor a mutation in *Unc93b1* (H412R) that abrogates endosomal TLR signaling (*8*). Consistently, patients with loss-of-function mutations in *UNC93B1* are highly susceptible to herpes encephalitis because of absent endosomal TLR function (*9*). In addition to its trafficking role, UNC93B1 has also been shown to be important for TLR5 function on the cell surface (*10*), maintenance of endosomal TLR expression and protein stability (*5*, *6*), and termination of TLR7 signaling via syntenin-1 (*11*).

Abnormally enhanced TLR7 signaling induced by aberrant immune recognition of self–nucleic acids has been shown to cause systemic autoimmunity in mice and humans (*11*–*17*). Notably, two distinct *Unc93b1* mutations (D34A and PKP530-532) that lead to TLR7 hyperactivation cause lupus-like features in mice (*11*, *15*), suggesting a role of UNC93B1 in selectively restraining aberrant TLR7 activation. Structural data on the UNC93B1/TLR7 complex suggest that UNC93B1 prevents TLR7 activation by inhibiting ligand-induced dimerization (*7*, *18*). However, the mechanisms that restrict premature or accidental activation of TLR7 remain unclear. Here, we describe missense *UNC93B1* variants that underlie uncontrolled TLR7 hyperactivation in patients with early-onset systemic lupus erythematosus (SLE).

RESULTS

UNC93B1 variants in patients with early-onset SLE

We investigated two siblings from a consanguineous family of Madeiran ancestry (family A; Fig. 1A). Patient 1 developed first symptoms of SLE at 4 months of age, including refractory autoimmune

[1]Department of Pediatrics, Medizinische Fakultät Carl Gustav Carus, Technische Universität Dresden, Dresden 01307, Germany. [2]Max Planck Institute for Infection Biology, Berlin 10117, Germany. [3]Gene Center, Systems Immunology, Ludwig-Maximilians-Universität Munich, Munich 81377, Germany. [4]Institute of Innate Immunity, University of Bonn, Bonn 53127, Germany. [5]Department of Microbiology and Immunology, Peter Doherty Institute for Infection & Immunity, University of Melbourne, Melbourne, VIC 3010, Australia. [6]Department of Pediatrics, Klinikum Dortmund, University Witten/Herdecke, Dortmund 44145, Germany. [7]Department of Pediatrics, Helios Klinik Krefeld, Krefeld 47805, Germany. [8]Department of Pediatric Respiratory Medicine, Immunology and Critical Care Medicine, Charité-Universitätsmedizin Berlin, Berlin 10117, Germany. [9]Deutsches Rheuma-Forschungszentrum (DRFZ), an institute of the Leibniz Association, Berlin 10117, Germany. [10]Berlin Institute of Health at Charité-Universitätsmedizin Berlin, Berlin 10178, Germany. [11]Department of Medicine, Rheumatology and Clinical Immunology, Charite-Universitätsmedizin Berlin, Berlin 10117, Germany. [12]Labor Berlin Charité-Vivantes GmbH, Department of Human Genetics, Berlin 13353, Germany. [13]Department of Cardiology and Nephrology, HELIOS Klinikum Berlin-Buch, Berlin 13125, Germany. [14]Institute of Virology, Technical University of Munich, Munich 81675, Germany. [15]Institute for Clinical Neuroimmunology, BioMedizinisches Zentrum, Ludwig-Maximilians-Universität Munich, Munich 82152, Germany. [16]German Center for Neurodegenerative Diseases (DZNE), Bonn 53175, Germany. [17]University Center for Rare Diseases, Medizinische Fakultät Carl Gustav Carus, Technische Universität Dresden, Dresden 01307, Germany.
*Corresponding author. Email: minae.lee-kirsch@uniklinikum-dresden.de

thrombocytopenia, autoimmune anemia, and erythematous rash, followed by hepatosplenomegaly, glomerulonephritis, arthritis, and panniculitis over the following 6 years; patient 2 presented with anemia, malar rash, renal disease, vasculitis, and seizures beginning at 2 years of age (tables S1 and S2). Both children exhibited multiple autoantibodies, including antinuclear antibodies (ANAs) and anti–double-stranded DNA (dsDNA), as well as strongly elevated IFN scores in peripheral blood mononuclear cells (PBMCs), as shown by increased expression of IFN-stimulated genes (Fig. 1B and tables S1 and S2). Levels of proinflammatory cytokines, IL-6, IL-8, and tumor necrosis factor–α (TNF-α), in sera and in media of cultured lymphoblastoid cells (LCLs) were markedly increased in both

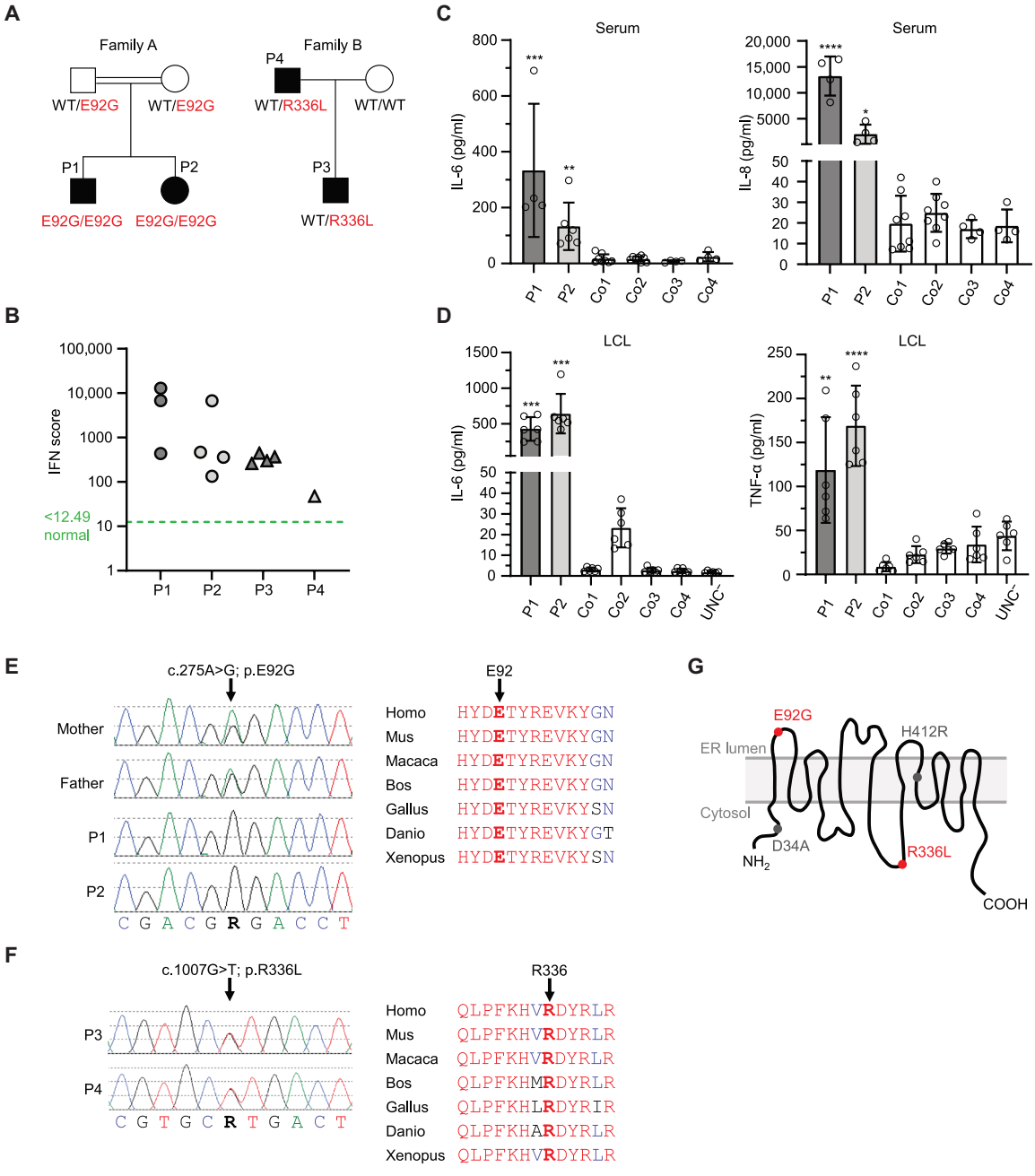

Fig. 1. Identification of *UNC93B1* mutations in two families with early-onset SLE. (**A**) Pedigrees of families with *UNC93B1* mutations. (**B**) IFN scores in PBMCs of patients (P1 to P4) based on quantitative RT-PCR. An IFN score of 12.49 (dashed green line) indicates the median IFN score of 10 healthy controls + 2 SD. (**C**) Levels of proinflammatory cytokines (IL-6 and IL-8) in patient sera, collected at different time points, compared with four healthy controls (Co1 to Co4). *$P < 0.05$; **$P < 0.01$; ***$P < 0.001$; ****$P < 0.0001$ versus mean of wild-type (WT) controls, Kruskal-Wallis test (Dunn's multiple comparison test) for IL-6 and one-way ANOVA (Dunnett's multiple comparison test) for IL-8. (**D**) Levels of IL-6 and TNF-α secreted by LCLs from two patients (P1 and P2), four wild-type controls (Co1 to Co4), and an UNC93B1-deficient individual (UNC$^-$). Means ± SD of at least four independent experiments. **$P < 0.01$; ***$P < 0.001$; ****$P < 0.0001$ versus mean of wild-type controls, Kruskal-Wallis test (Dunn's multiple comparison test). (**E** and **F**) Electropherograms showing *UNC93B1* mutations and multiple sequence alignment indicate high conservation of E92 (E) and R336 (F) of the UNC93B1 protein. (**G**) Schematic of UNC93B1 topology depicting human mutations (E92G and R336L) and mouse mutations D34A (gain of function) and H412R (loss of function). ER, endoplasmic reticulum.

patients (Fig. 1, C and D), compared with wild-type controls and a previously reported UNC93B1-deficient control (*9*). Whole-exome sequencing revealed a homozygous variant in *UNC93B1* (c.275A>G, p.E92G; NM_030930.4) in both children affecting a highly conserved amino acid residue located within the first luminal loop (Fig. 1, E to G). Both healthy parents were heterozygous carriers of the E92G variant that was reported once in the gnomAD database and predicted to impair function (Fig. 1E and table S3).

The second family (family B) is of European German ancestry (Fig. 1A). The son, patient 3, presented first signs of SLE at 18 months of age, including dermatitis, positive ANAs, and hypocomplementemia. At 16 years, he developed hepatomegaly, progressive generalized lymphadenopathy, and arthralgia. At 19 years, he was noted to have proteinuria, hyperglobulinemia, anti–β_2-glycoprotein, and anti-dsDNA antibodies (tables S1 and S2). His father, patient 4, presented first symptoms at 5 years of age, including malar rash, photosensitivity, arthralgia, and positive ANAs. At 30 years, he developed lupus nephritis (Fig. 1A and tables S1 and S2). Similar to the patients of family A, both affected members of family B exhibited strong IFN signatures and elevated proinflammatory serum cytokines (Fig. 1B and fig. S1). Whole-exome sequencing led to the identification of a heterozygous previously undescribed *UNC93B1* variant (c.1007G>T, p.R336L), which is highly conserved and predicted to be damaging (Fig. 1, E to G, and table S3). In both families, no other mutations, including variants of unknown importance, or copy number variants in genes previously implicated in autoimmune lymphoproliferative syndrome or other monogenic forms of lupus were found.

SLE-associated transcriptional signatures in patient cells

To study the transcriptional changes related to *UNC93B1*^{E92G} in a cell type–resolved manner, we performed single-cell RNA (scRNA) sequencing in PBMCs from patient 1 and a sex- and age-matched healthy control. A total of 3354 and 5906 cells for patient 1 and control, respectively, were retained for analysis after filtering out doublets and low-quality cells. We annotated nine distinct cell types covering all expected cell types (Fig. 2, A to C). Consistent with migration of plasmacytoid dendritic cells (pDCs) into tissues upon activation by self–nucleic acid–containing immune complexes (*19*, *20*), pDCs were underrepresented in the patient sample (Fig. 2B). In line with clinical data (table S4) and previous single-cell data from patients with SLE (*21*), there was a reduction of $CD4^+$ helper T cells and an expansion of cytotoxic $CD8^+$ T cells (Fig. 2B). Likewise, $CD8^+$ T cells exhibited a cytotoxic signature (*PRF1*, *GZMH*, and *GZMB*) and an exhaustion signature (*PDCD1*, *CTLA4*, *LAG3*, *CD160*, *TIGIT*, *HAVCR2*, and *CD244*), in addition to a generally increased IFN signature (Fig. 2, D and E). Patient cells exhibited elevated expression of IFN-stimulated genes (ISGs) across all cell types but most prominently in monocytes and dendritic cells (Fig. 2D). Differential gene expression analysis and gene ontology (GO) term enrichment analysis revealed cell type–specific transcriptional responses in patient cells compared with the control, including activation of B cells in terms of cell cycle regulation (GO:0051726), up-regulation of IL-12 signaling (GO:0071349) in $CD4^+$ T cells, and induction of IFN-γ (GO:0032729) and TNF-α (GO:0010803) in $CD8^+$ T cells, indicative of T cell activation (Fig. 2F). Similar to children with complex SLE (*19*), $CD8^+$ T cells, natural killer (NK) cells, and $CD16^+$ monocytes exhibited a distinct IL-1β signature (GO:0050718), whereas $CD14^+$ and $CD16^+$ monocytes featured a response to lipopolysaccharide (LPS) (GO:0032496), with up-regulation of NF-κB in $CD16^+$ monocytes (GO:0051092) (Fig. 2F).

To assess the general validity of the transcriptional cellular phenotypes observed in patient 1 and to gain further insight into rare cell subtypes, we assessed fluorescence-activated cell sorting (FACS)–sorted PBMCs (enriched for T cells, B cells, monocytes, and pDCs) of patient 3 who carries the *UNC93B1*^{R336L} mutation (fig. S2, A to D). These orthogonal data largely confirmed the cell type–specific transcriptional phenotypes described for patient 1, in particular, the IFN signature and cytotoxic phenotype in $CD8^+$ T cells (fig. S2, B and C). Furthermore, peripheral B cells from patient 3 showed an increase in $CD27^{high}CD38^{high}$ plasmablasts compared with healthy controls (fig. S3), consistent with enhanced B cell hyperreactivity, and an increase in double-negative $CD27^-IgD^-$ B cells (fig. S3), a distinct memory B cell subset commonly expanded in SLE (*16*, *22*). Collectively, these findings indicate that cell type–specific transcriptional signatures and B cell phenotypes of the patients carrying *UNC93B1* mutations are highly similar to those observed in complex SLE.

Constitutive activation of ssRNA-sensing TLRs in patient cells

Given the essential role of UNC93B1 for endosomal TLR function and the observed chronic type I IFN activation in the patients, we hypothesized that the identified *UNC93B1* mutations might underlie hyperactivation of TLR-dependent nucleic acid–sensing pathways. To investigate the signaling properties of UNC93B1-dependent TLRs in patient cells, we measured cytokine responses using specific agonists. After stimulation with R848, an imidazoquinoline compound with TLR7/TLR8 agonist activity, patient PBMCs (P1 and P2) produced markedly higher levels of TNF-α compared with wild-type controls (Fig. 3A). In contrast, IFN-γ–inducible protein 10 (IP-10) secretion by PBMCs in response to the TLR9 agonist ODN2006 and IL-8 secretion by primary fibroblasts in response to the TLR3 agonist polyinosinic-polycytidylic acid [poly(I:C)] did not differ between patients and controls (Fig. 3A). Likewise, patient LCLs also produced much higher amounts of IL-6 and TNF-α, both at basal level and in response to R848, than LCLs from wild-type controls or a patient carrying a loss-of-function *UNC93B1* mutation (*9*), whereas patient LCLs showed normal responses to ODN2006 (Fig. 1D and fig. S4, A and B). Stimulation of UNC93B1-independent TLR2 (Pam2CSK4) in LCLs or TLR4 (LPS) in fibroblasts did not reveal any differences in cytokine secretion between patients and controls (fig. S4, C and D). To further assess TLR7-specific hyperactivation, we stimulated whole blood of patients carrying either the *UNC93B1*^{E92G} or the *UNC93B1*^{R336L} mutation with selective agonists. Treatment with the TLR7 agonist R837 resulted in a strong IL-6 production by patient cells compared with wild-type controls (fig. S5), corroborating TLR7 hyperactivation. Although patient cells also displayed hyperresponsiveness to the TLR8 agonist TL8-506, their cytokine response to the TLR9 agonist ODN2216 did not differ from wild-type controls (fig. S5).

Similar to R848, endosomal delivery of RNA40, a well-established 20-nucleotide oligomer ssRNA ligand specific for TLR7/TLR8 (*23*), resulted in a much higher TNF-α secretion in patient PBMCs than in controls (fig. S6). The presence of hydroxychloroquine (HCQ), an antimalarial drug that impedes nucleic acid recognition by endosomal TLRs (*24*), reduced signaling in both wild-type and mutant cells (fig. S6), consistent with hyperactivation of TLR7/8 in endosomes. Moreover, we observed similar ratios of full-length and cleaved TLR7 in LCLs from both patients carrying the *UNC93B1*^{E92G} mutation and wild-type controls (Fig. 3B). Because cleavage of full-length TLR7 occurs within the acid environment of the endosome, this further

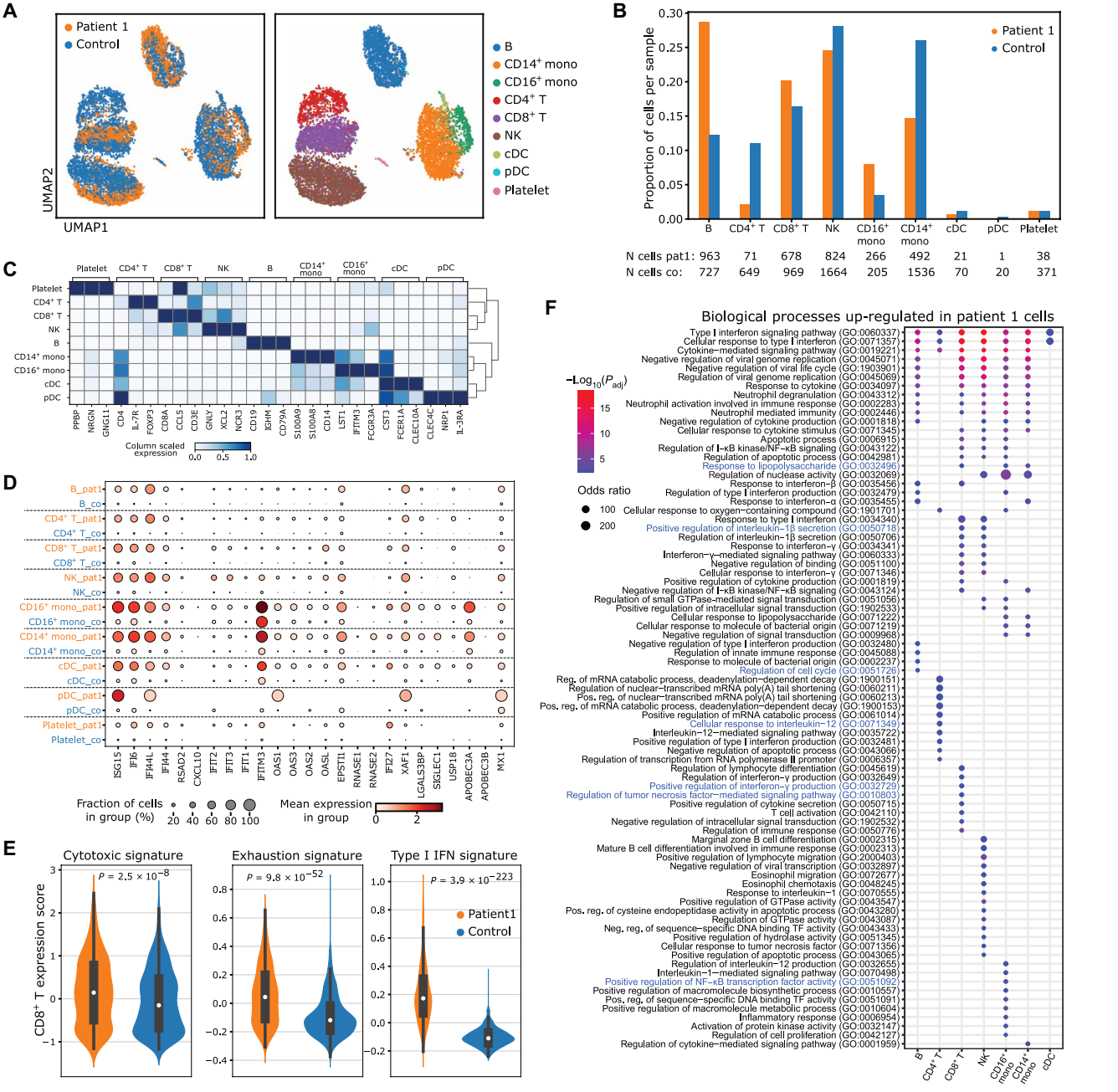

Fig. 2. scRNA sequencing of PBMCs of patient 1 and control. (**A**) Integrated uniform manifold approximation and projection (UMAP) of data from patient 1 and one age- and sex-matched control, assigned to nine cell subtypes: B, B cells; mono (CD16$^+$ and CD14$^+$), monocytes; T (CD8$^+$ and CD4$^+$), T cells; NK cells; cDC, conventional dendritic cells; pDCs; platelets. (**B**) Bar graph displaying the individual cell type proportions in patient 1 and control, with corresponding absolute cell numbers. (**C**) Heatmap displaying relative marker gene expression across cell types. (**D**) Dot plot showing cell type–specific ISG expression. (**E**) Violin plots depicting cytotoxic, exhaustion, and IFN signatures in CD8$^+$ T cells, comparing patient and control cells. Two-sided Wilcoxon rank sum test. (**F**) Dot plot showing the GO terms that are enriched in genes overexpressed in the patient cells compared with control cells for each of the indicated cell types. Two-sided Fisher's exact test corrected for multiple testing (false discovery rate). GTPase, guanosine triphosphatase; poly(A), polyadenylate; TF, transcription factor.

demonstrates that TLR trafficking as such is not affected by the *UNC93B1*^{E92G} mutation.

IFN-α up-regulates TLR7 expression in B cells, promotes cell death and release of self–nucleic acids, and primes pDCs to respond more effectively to immune complexes (*25*, *26*). Accordingly, TLR7 expression in patient 1 was slightly up-regulated only in B cells but not in any of the other assessed PBMC cell types, whereas in patient 3, TLR7 was slightly up-regulated in B cells, monocytes, and pDCs but not correlated with *IFNA1* or *ISG15* gene expression (fig. S7, A to D). We also confirmed that pDCs, the main IFN-α–producing cells able to secrete up to 1000 times more type I IFNs than any other white blood cell, did not substantially express TLR8 (*27*, *28*) in either patient (fig. S7, A and C). Together, these findings suggest that type I IFN activation in patients carrying the *UNC93B1*^{E92G} or

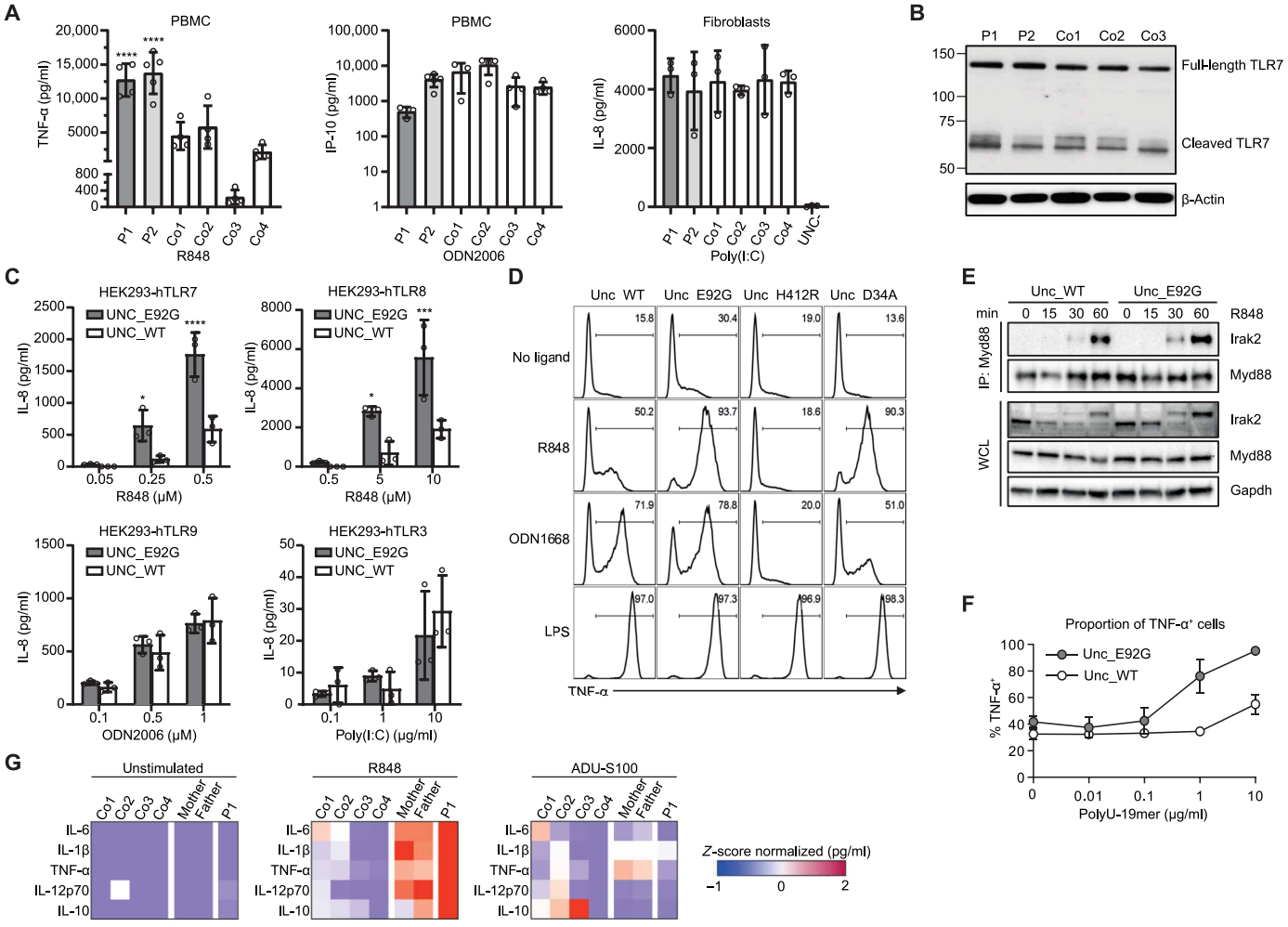

Fig. 3. Functional consequences of the UNC93B1^{E92G} mutation on TLR signaling. (**A**) Secretion of TNF-α and IP-10 by PBMCs after stimulation with the TLR7/8 agonist R848 (1 μg/ml) or the TLR9 agonist ODN2006 (0.5 μM) and secretion of IL-8 by fibroblasts after stimulation with the TLR3 agonist poly(I:C) (10 μg/ml). Controls (Co1 to Co4), UNC93B1-deficient control (UNC$^-$). Means ± SD of at least three technical replicates. One-way ANOVA (Dunnett's multiple comparison test). ****$P < 0.0001$ versus controls. (**B**) Expression of full-length and cleaved TLR7 in LCLs. β-Actin was probed as loading control. (**C**) Secretion of IL-8 by TLR-expressing HEK293 cells transduced with mutant (UNC_E92G) or wild-type (UNC_WT) UNC93B1 using the indicated agonists. Means ± SD of three technical replicates. Two-way ANOVA (Bonferroni's multiple comparison test). *$P < 0.05$; ***$P < 0.001$; ****$P < 0.0001$ versus UNC_WT. (**D**) Production of TNF-α in *Unc93b1*$^{-/-}$ mouse RAW264.7 macrophages reconstituted with Unc93b1 variants stimulated with the indicated TLR agonists. (**E**) Myddosome formation assayed by coimmunoprecipitation (IP) of whole-cell lysates (WCL) from Unc93b1-reconstituted *Unc93b1*$^{-/-}$ RAW264.7 cells using anti-Myd88 antibody, followed by Western blot analysis using anti-Irak2 antibody. Gapdh was immune-stained as loading control. (**F**) Proportion of TNF-α–positive cells in Unc93b1-reconstituted *Unc93b1*$^{-/-}$ RAW264.7 cells after stimulation with polyU-ssRNA. Means ± SD of four technical replicates. Data are representative of at least three (A to C) or two (D to F) independent experiments. (**G**) Heatmap of inflammatory cytokines after stimulation of whole blood from Co1 to Co4 and P1 and his parents (mother and father) with R848 and ADU-S100.

UNC93B1^{R336L} mutation is likely caused by hyperactivation of the TLR7 signaling pathway that is not due to an increased expression of *TLR7*.

Recapitulation of TLR7 hyperactivation in human embryonic kidney–293 cells and mouse macrophages

To further exclude that hyperactivation of ssRNA-sensing TLRs observed in *UNC93B1*^{E92G} patient cells was caused by up-regulation of TLR7/TLR8 due to systemic type I IFN activation, we studied human embryonic kidney (HEK) 293 cells with stable expression of endosomal TLRs. To facilitate endosomal targeting and signaling of TLRs (*4*), we coexpressed UNC93B1. TLR-expressing HEK293 cells were transduced with citrine-tagged UNC93B1 variants and sorted by flow cytometry to ensure equal expression (fig. S8). In HEK293 cells expressing either TLR7 or TLR8 (HEK293-hTLR7 and HEK293-hTLR8), stimulation with R848 markedly increased IL-8 secretion in the presence of the E92G mutant compared with cells expressing wild-type UNC93B1 (Fig. 3C). Similarly, endosomal delivery of RNA40 to HEK293-hTLR7 led to higher IL-8 production in the presence of mutant UNC93B1 compared with wild-type UNC93B1, which was reduced by HCQ (fig. S9A). In contrast, stimulation of HEK293-hTLR9 or HEK293-hTLR3 with their cognate ligands, ODN2006 or poly(I:C), respectively, or endosomal delivery of ODN2006 to HEK293-hTLR9 led to comparable IL-8 production, irrespective of the presence of mutant or wild-type UNC93B1 (Fig. 3C and fig. S9B).

We next investigated TLR signaling in transgenic RAW 264.7 *Unc93b1*$^{-/-}$ murine macrophages stably expressing equal levels of

mouse *Unc93b1* variants (E92G, D34A, and H412R; fig. S10A). No difference in Tlr7 expression was observed in *Unc93b1*$^{-/-}$ murine macrophages reconstituted with *Unc93b1* variants (fig. S10A). In response to R848 stimulation, TNF-α production in cells carrying the E92G mutation was significantly stronger compared with cells expressing wild-type Unc93b1 (Fig. 3D). This was accompanied by enhanced Myddosome formation, the most proximal signaling step downstream of TLR7 activation, as shown by recruitment and posttranslational modification of IL-1 receptor–associated kinase (Irak2) (Fig. 3E). In contrast, no differences were observed when cells were stimulated with the TLR9 ligand ODN1668 (Fig. 3D), confirming a TLR7-specific activating effect conferred by the *Unc93b1*^{E92G} variant. As expected, in presence of the loss-of-function mutant *Unc93b1*^{H412R}, which abrogates function of all endosomal TLRs (*8*), no immunostimulatory response was observed (Fig. 3D). Notably, cells expressing the known activating *Unc93b1*^{D34A} mutation identified in the mouse (*15*) also showed an enhanced TNF-α secretion in response to R848, whereas TNF-α secretion in response to ODN1668 was reduced (Fig. 3D), consistent with the previously reported inverse effect of D34A on TLR7 and TLR9 signaling (*15*, *29*). Enhanced TLR7 signaling in *Unc93b1*^{E92G}-expressing mouse macrophages was confirmed using the ssRNA-analog polyuridine (Fig. 3F). Collectively, these findings demonstrate that *Unc93b1*^{E92G} confers a gain of function, selectively leading to TLR7/8, but not TLR3 or TLR9, hyperactivation.

The UNC93B1^{E92G} allele confers an additive gain of function

In contrast to the affected members of family B who harbor a dominantly inherited heterozygous *UNC93B1*^{R336L} variant, both affected children of family A carry a homozygous *UNC93B1*^{E92G} mutation, raising the question as to the phenotypic effects conferred by *UNC93B1*^{E92G}. Given that gain-of-function mutations are usually dominant, we sought to investigate whether the parents of patient 1 and patient 2 (family A), both of whom are healthy heterozygous carriers of the *UNC93B1*^{E92G} variant, exhibit an intermediate phenotype. To this end, we assessed induced cytokine responses in whole blood after stimulation with the TLR7/TLR8 agonist R848 and the stimulator of interferon genes (STING) agonist ADU-S100, respectively. Stimulation of whole blood with R848 resulted in a strong proinflammatory response in both parents compared with healthy controls, with increased production of IL-6, IL-1β, and TNF-α (Fig. 3G). This inflammatory response, however, was not as pronounced as in their affected child (P1; Fig. 3G), despite the fact that he was under treatment with a Janus kinase (JAK) inhibitor at the time of blood withdrawal and had proinflammatory cytokines within normal range at baseline. Notably, similar to patient 1, both his parents were also less responsive to stimulation with the STING agonist ADU-S100, compared with controls (Fig. 3G), consistent with a negative regulatory role of STING signaling on TLR-dependent autoimmunity (*30*). Thus, *UNC93B1*^{E92G} appears to be semidominant and has a gene dosage effect with large phenotypic effects in homozygous individuals and weaker effects in heterozygous carriers.

UNC93B1^{E92G} destabilizes the interaction with TLR7

Recent data on the cryo–electron microscopy structures of TLR7 in complex with UNC93B1, which assembles as a dimer with a 2:2 stoichiometry, have shown that both TLR monomers interact with the UNC93B1 N-terminal six-helix bundle through their transmembrane and luminal juxtamembrane regions (*7*). Notably, the overlay of the UNC93B1/TLR7 structure in the absence of ligand onto the TLR7 ectodomain structure in the ligand-bound state revealed a steric clash between the two UNC93B1 molecules because of the tilt angle imposed by the ectodomains (*7*, *18*), suggesting that UNC93B1 may prevent TLR7 activation by keeping it in an inactive conformation. To explore this further, we examined the consequences of E92G on UNC93B1 structure. Notably, the E92G mutation lies within the two-turn helix (H1) formed between UNC93B1 transmembrane domain 1 (TM1) and TM2 (residues 91 to 97) (Fig. 4A). This region was shown to make contact with the two loop regions of the C-terminal LRR-CT motif of the TLR7 ectodomain and to confer rigidity to the orientation of the LRR-CT motif (*3*, *7*). Structural analysis revealed that the E92G mutation on H1 of UNC93B1 may disrupt potential electrostatic interactions of E92 with nearby residues in the TM5-TM6 loop of UNC93B1, such as K273 (*7*) (Fig. 4A). This is the most extended luminal loop of UNC93B1, and disruption of these stabilizing interactions may lead to an increased flexibility of the loop or affect glycosylation of neighboring residues N272 and N251 that are also located on the TM5-TM6 loop (Fig. 4A). Thus, the mutation E92G could potentially lead to destabilization of the UNC93B1 protein.

The R336L mutation lies within the intracellular helix H3 formed between UNC93B1 TM6 and TM7 at the interface of the UNC93B1 dimer that keeps the two TLR7 monomers at a distance and prevents dimerization of the TIR domains (Fig. 4B), the initiating step of TLR7 signaling. Notably, R336 is in close proximity to K333, which was recently shown to undergo ubiquitylation in the context of TLR7 signaling termination (*11*). Accordingly, K63-linked ubiquitylation of UNC93B1 along with syntenin-1 recruitment is critical for termination of TLR7 signaling by sorting of UNC93B1/TLR7 into intraluminal vesicles (*11*). As such, UNC93B1^{R336L} could either interfere with the inhibitory function of UNC93B1 on TLR7 signaling or impede TLR7 signaling termination, thereby leading to TLR7 hyperactivation.

To further investigate UNC93B1^{E92G} protein stability, we measured levels of wild-type and mutant citrine-tagged UNC93B1 expressed in HEK293 cells after sorting to equal citrine fluorescence intensity ($t = 0$ hours). Compared with wild-type UNC93B1, protein levels of the E92G mutant measured at 6 and 24 hours were lower (Fig. 4C), indicating reduced protein stability. To assess the impact of E92G on the interaction of Unc93b1 with endosomal Tlrs, we transduced Flag-tagged Unc93b1-reconstituted *Unc93b1*$^{-/-}$ RAW264.7 macrophages with hemagglutinin (HA)–tagged Tlr3, Tlr9, and Tlr7, respectively. Despite equal Tlr expression levels, Unc93b1^{E92G} interacted less with Tlr7 compared with wild-type Unc93b1, as shown by coimmunoprecipitation of Flag-tagged Unc93b1, whereas the interaction with Tlr3 and Tlr9 was not altered (Fig. 4D). Similarly, Flag-tagged Unc93b1 interacted less with endogenous Tlr7 (fig. S10B). Thus, although Unc93b1^{E92G} was able to interact with Tlr7, this interaction was less stable. This is in contrast to the H412R loss-of-function *Unc93b1* mutant, which abolishes interaction with endosomal Tlrs (fig. S10B) (*5*). Given that ligand binding occurs within the concave side of the horseshoe-shaped ectodomain of TLR7, these findings suggest that a reduced interaction of UNC93B1 with TLR7 due to destabilization of UNC93B1 increases binding site accessibility.

To explore whether disturbed syntenin-1–mediated termination of TLR7 signaling (*11*) could account for TLR7 hyperactivation observed in our patients, we examined syntenin-1 recruitment to UNC93B1 in response to TLR7 stimulation in HEK293 cells stably expressing TLR7 and equal levels of citrine-tagged UNC93B1 variants.

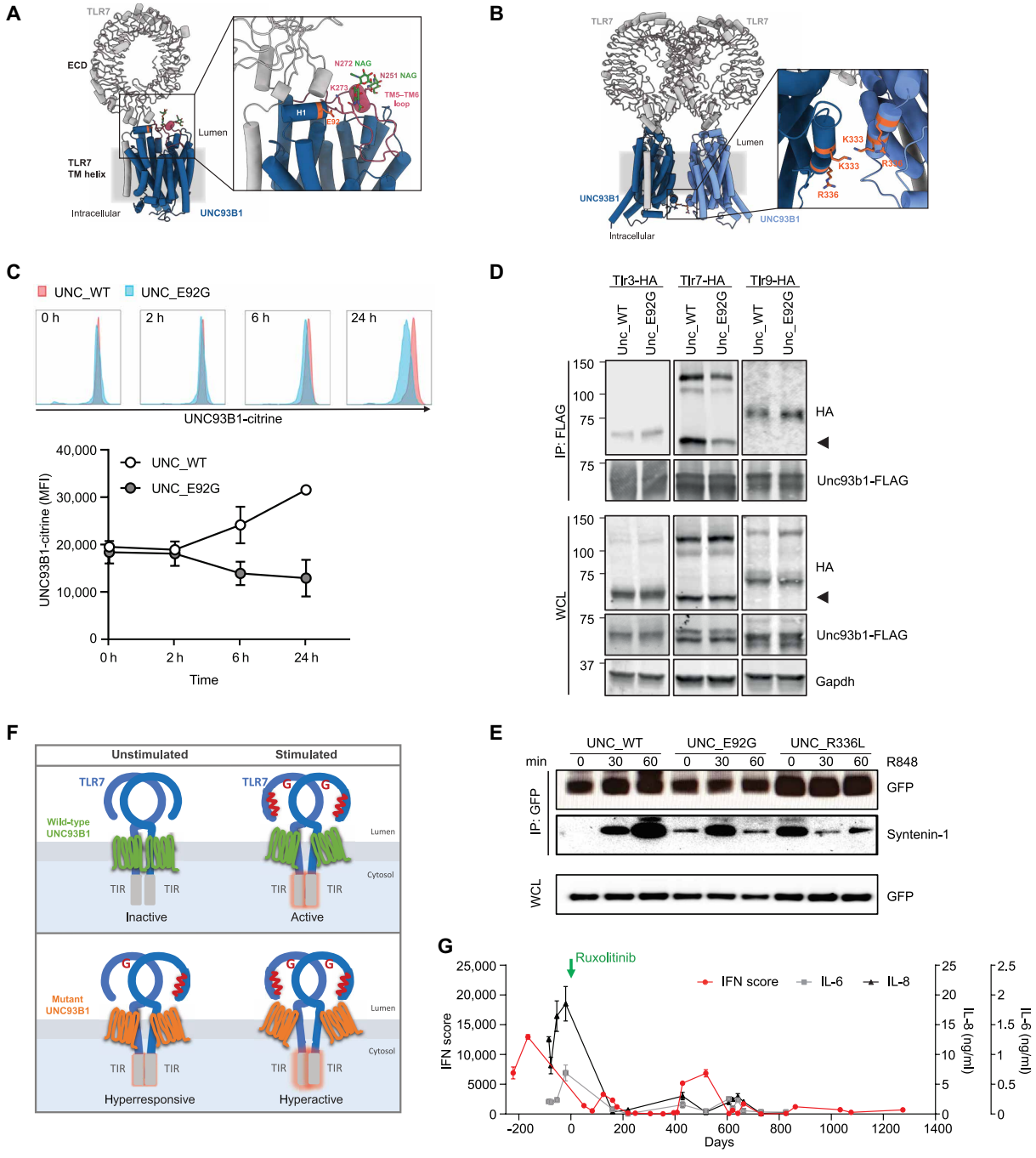

Fig. 4. UNC93B1 stability, interaction of UNC93B1 with TLR7 and syntenin-1, and effect of ruxolitinib treatment on inflammatory markers. (**A**) Structure of TLR7 (gray) bound to UNC93B1 (blue) with residue E92 colored in orange (PDB 7CYN). Close-up view of residue E92 on H1 of UNC93B1 and its close proximity to residue K273 on the UNC93B1 TM5-TM6 luminal loop (pink). Glycosylation of residues N272 and N251 is depicted in dark green. TM, transmembrane. ECD, extracellular domain. (**B**) Structure of TLR7 (gray)–UNC93B1 (blue) dimer. Close-up view of residue R336 and its close proximity to residue K333 on the UNC93B1 TM6-TM7 intracellular loop. UNC93B1 monomers are shown in light and dark blue. (**C**) Stability of wild-type (red) and mutant (blue) citrine-tagged UNC93B1-expressing HEK293 cells over time, as measured by flow cytometry (top). Quantification of mean fluorescence intensity (MFI) of citrine-tagged UNC93B1-expressing cells at indicated time points (means ± SD; $n = 3$; bottom). (**D**) Coimmunoprecipitation of whole-cell lysates from *Unc93b1*$^{-/-}$ RAW264.7 cells reconstituted with Flag-tagged Unc93b1 variants using anti-Flag antibody (IP:Flag), followed by Western blot analysis using anti-HA antibody. Arrow heads indicate active TLR7. Representative data of two independent experiments. (**E**) Coimmunoprecipitation of whole-cell lysates from HEK293 cells stably expressing TLR7 and equal levels of citrine-tagged UNC931 variants stimulated with R848 using anti-GFP antibody (IP:GFP), followed by Western blot analysis using anti–syntenin-1 antibody. Representative data of two independent experiments. (**F**) Model depicting how structural changes imposed by *UNC93B1* mutations could either modify the ligand-binding properties of TLR7 by enhancing binding site accessibility (E92G) or promote signaling initiation by facilitating TIR domain dimerization (R336L), resulting in hyperresponsiveness and hyperactivity of the TLR7 receptor. (**G**) IFN scores and levels of proinflammatory cytokines in blood of patient 1 during treatment with ruxolitinib. Day 0 indicates the start of ruxolitinib treatment.

Notably, *UNC93B1*^{R336L} lies on the intracellular side where syntenin-1–binding takes place, whereas *UNC93B1*^{E92G} localizes on the luminal side of the endosome away from the syntenin-1–binding region (Fig. 4A). While wild-type UNC93B1 did not bind to syntenin-1 in the absence of TLR7 stimulation, treatment with R848 led to rapid syntenin-1 recruitment within 30 min, which further increased over 60 min, as shown by coimmunoprecipitation of citrine-UNC93B1 (Fig. 4E), confirming this mechanism of TLR7 signaling termination by syntenin-1 also in human cells. Notably, both UNC93B1 mutants showed an association with syntenin-1 already in the absence of R848 stimulation (Fig. 4E), consistent with constitutive activation of TLR7 signaling termination due to TLR7 activation at steady state in patient cells. Both UNC mutants, however, exhibited distinct dynamics of syntenin-1 recruitment. Syntenin-1 binding to UNC93B1^{E92G} was low at baseline, increased at 30 min upon R848 stimulation, and subsided to baseline levels after 60 min (Fig. 4E). In contrast, the level of syntenin-1 recruitment to UNC93B1^{R336L} at baseline already exceeded that of wild-type UNC93B1 at 30 min of R848 stimulation. After R848 stimulation, syntenin-1 binding to UNC93B1^{R336L} did not further increase but, instead, was markedly reduced at 30 min with only little increment after 60 min (Fig. 4E). These findings indicate that chronic TLR7 hyperactivation causes concomitant activation of syntenin-1–dependent signaling termination, which may result in syntenin-1 consumption. Accordingly, TLR7 signaling termination via syntenin-1 per se is not impaired by the *UNC93B1* mutations, although syntenin-1 exhaustion may contribute to TLR7 hyperactivation. Together, our findings delineate a pivotal role for UNC93B1 in preventing autoimmunity by restraining uncontrolled TLR7 activation (Fig. 4F).

Therapeutic response of patient 1 to JAK1/2 inhibition

JAK1/2 inhibitors such as ruxolitinib dampen type I IFN activity by impeding IFN-α/β receptor signaling. Consistently, spontaneous type I IFN signaling in whole blood of patient 1 was efficiently suppressed by ruxolitinib in vitro (fig. S11). Given the refractory course of the disease and the very high IFN signature, patient 1 was started on ruxolitinib, which led to a sustained suppression of systemic type I IFN activation with decreased serum levels of IL-8 and IL-6 (Fig. 4G and table S1). This was accompanied by amelioration of transfusion-dependent anemia, panniculitis, and renal disease. However, despite significant clinical improvement, the boy continued to experience flares with systemic inflammation and renal dysfunction (table S1). Several attempts to increase the dose of ruxolitinib to 1 mg/kg to achieve more effective type I IFN inhibition were associated with cytopenia, a known side effect of JAK1/2 inhibitors. Thus, although JAK inhibition is of therapeutic value in patients with TLR7 hyperactivation due to *UNC93B1* mutation, our clinical observations in this patient also reveal a limitation of this approach and highlight the need for more specific TLR7-targeting therapies.

DISCUSSION

We delineate a monogenic form of SLE caused by mutation in *UNC93B1* that confers a gain of function due to hyperactivation of TLR7 signaling. Engagement of TLR7 by self-RNA derived from endocytosed microbial particles or apoptotic cells initiates downstream signaling pathways resulting in the production of IFN-α and proinflammatory cytokines. In SLE, IFN-α drives a self-perpetuating feedback loop that promotes the loss of tolerance and autoimmunity in a non–cell-autonomous manner (*26*). The clinical and cellular phenotype of the patients resembled that reported for mice carrying the D34A or the PKP530-532 gain-of-function *Unc93b1* mutations, which succumb to TLR7-dependent autoimmunity (*11*, *15*). Our findings in patient cells indicate enhanced activation of ssRNA-sensing TLR7 and TLR8. However, *TLR8* gain-of-function mutations were recently shown to cause increased susceptibility to infections associated with neutropenia and hypogammaglobulinemia (*31*), whereas a *TLR7* gain-of-function mutation causes SLE (*17*). In contrast, the patients with SLE carrying *UNC93B1* variants had normal neutrophils and exhibited autoimmunity with hypergammaglobulinemia and increased memory-switched B cells, consistent with enhanced B cell hyperresponsiveness caused by TLR7 hyperactivity (tables S1 and S4). Notably, although *TLR8* is predominantly expressed in neutrophils, expression of *TLR7* is restricted to B cells and pDCs in humans (*32*). This may explain why *TLR8* gain-of-function mutations are associated with neutropenia and infections. Given the pivotal role of B cells and dendritic cells in SLE pathogenesis, this suggests that autoimmunity in our patients is primarily driven by increased TLR7 signaling.

TLR7 harbors two spatially distinct ligand-binding sites within the horseshoe-shaped LRR-CT motif—a first site for guanosine and a second site for short ssRNA (*18*). Moreover, TLR7 exhibits a synergistic mode of activation in response to its two ligands, whereby successive ligand binding increases binding affinities (*18*, *33*, *34*). Similarly, TLR8 was shown to harbor two binding sites for uridine and ssRNA degradation products (*28*, *35*). Notably, host-derived nucleases are not able to fully degrade RNA ligands to prevent self–nucleic acid recognition by TLR7 or TLR8 (*28*, *36*). Given that nucleosides, such as guanosine and uridine, are essential primary metabolites in all living cells, these findings indicate that nucleosides and endogenous degradation products of ssRNA represent natural small TLR7/8 ligands. We propose that engagement of such endogenous ligands dictates TLR7 activity at steady state and thus fine-tunes the general alertness of the TLR7 sensing system under the control by UNC93B1. Because binding of both ligands is required for full receptor activation, binding site accessibility critically affects ligand engagement. Moreover, TLR7 signaling depends on proper dimer assembly, and ligand binding induces a conformational change that reorients the TIR domains to initiate signaling, a process that likely involves some form of dissociation of TLR7 from UNC93B1 (*7*). Consequently, a loss of structural rigidity that loosens the tight interaction between UNC93B1 and TLR7 could therefore modify the ligand-binding properties of TLR7 by enhancing binding site accessibility (E92G) or promoting signaling initiation by facilitating TIR domain dimerization (R336L). As a result, both UNC93B1 mutations alter the steady state of TLR7 activation toward a higher responsiveness (Fig. 4F). By demonstrating that E92 is important not only for UNC93B1 stability but also for its interaction with TLR7, we provide further insight into the mechanisms by which the UNC93B1-TLR interaction coordinates TLR signaling. Thus, ligand-binding properties of TLRs appear to be dependent on conformational restraints exerted by UNC93B1 on the receptor. Consistent with this notion, an *Unc93b1* mutant that greatly enhances interaction with TLR9 was recently shown to attenuate ligand binding, thereby impeding signaling (*37*). The inverse logic might apply to the E92G mutant, in which reduced interaction with TLR7 promotes responsiveness. As such, the association strength of UNC93B1 might be a general predictor of TLR responsiveness, whereby increased affinity restricts receptor activity, whereas reduced affinity liberates activity. The

differential effects of E92G on endosomal TLRs may reflect subtype-specific variations in the contact sites with UNC93B1 and the resulting positioning of the ligand-binding sites, suggesting that UNC93B1 controls TLR subtype–specific mechanisms of ligand recognition. In line with TLR subtype–specific functions of UNC93B1, a recently reported glutamic acid insertion (p.Glu49dup) in the UNC93B1 N terminus that selectively impairs the degradative sorting of TLR7, leading to endosomal receptor accumulation, is also associated with human lupus (*38*).

scRNA sequencing of PBMCs from patient 1 and patient 3, harboring two different *UNC93B1* mutations, revealed alterations in cell type composition and dysregulated transcriptional networks that are also observed in patients with complex SLE (Fig. 2 and fig. S2). As such, our findings are of particular clinical relevance regarding the management of patients with SLE, patient stratification for clinical trials, and drug development. Unlike JAK inhibitors, which inhibit type I IFN signaling at the level of the IFNAR receptor, TLR7 antagonists target uncontrolled type I IFN activation more upstream at the site where the disease-causing immune signaling is primarily initiated. Given that such TLR7 inhibitory molecules have already been developed and tested preclinically (*39*, *40*), our findings support accelerating further development of TLR7 antagonists for patients with SLE. Although *UNC93B1* variants have not previously been implicated in human susceptibility to SLE, a genetic association of an *Unc93b1* variant with cutaneous lupus was recently demonstrated in dogs (*41*), suggesting that rare variants in human *UNC93B1* may also contribute to the risk for complex SLE.

MATERIALS AND METHODS

Study design

In this study, we enrolled four patients with early-onset SLE from two unrelated families. We collected blood and serum samples for genetic and immunologic investigations. LCLs and primary fibroblasts derived from skin biopsies were established for functional analysis. Written informed consent was obtained by all participating members of the families or their legal guardians. The study was approved by the ethics committees of the Medical Faculty, Technische Universität Dresden, and Charité-Universitätsmedizin Berlin and conducted in accordance with the Declaration of Helsinki.

Whole-exome sequencing

Genomic DNA was extracted from blood using QIAamp DNA Blood Mini Kit (QIAGEN). For family A, whole-exome sequencing was carried out as previously described (*42*). Constructed exome libraries were subjected to Illumina HiSeq4000/Xten (Illumina) 150–base pair paired-end sequencing with an average read depth of 134.5. SOAPnuke was used to remove adapter sequences, low-quality reads, and N reads (*43*). Sequences were mapped to the human reference genome (GRCh37/UCSC hg19) by Burrows-Wheeler algorithm (BWA-MEM, version 0.7.10) (*44*). GATK Haplotype Caller (version 3.3) (*45*) was used for single-nucleotide variants and insertions/deletions calling and Ensembl VEP (variant effect predictor) (*46*) for annotation. For family B, whole-exome sequencing was performed following library preparation (SureSelect Human All Exon V6, Agilent) as paired-end next-generation sequencing (Illumina Inc., CA, USA). Generated sequence data were analyzed using the Labor Berlin in-house next-generation sequencing data analysis pipeline (v1.0) and compared with the human reference sequence (hg19). Variant prioritization was based on allele frequency, variant type, location in the gene, bioinformatic prediction tools, biological function, and evidence from literature using VarFish (*47*) and MutationDistiller (*48*).

Sanger sequencing

Genomic DNA flanking the *UNC93B1* (NC_000011) mutation was amplified by polymerase chain reaction (PCR) using gene-specific primers [Eurofins MWG Operon; E92, GAATGCCTTCGGTGATTGGAG (forward) and GTTCCTGTTTCCTTCCCCAAATC (reverse); R336, GAGCGGAAACCTCATTGTGG (forward) and CGATACCAGTGCAGGCAAAG (reverse)] and sequenced in both directions using the BigDye Terminator v1.1 Cycle Sequencing Kit (Applied Biosystems) on a 3130xl genetic analyzer (Applied Biosystems). Data were analyzed using Vector NTI software (Life Technologies).

Flow cytometry staining

PBMCs were isolated from EDTA-anticoagulated whole blood using Ficoll density centrifugation and stained with the following anti-human antibodies: CD14 (M5E2, BUV395, BD Biosciences, catalog no. 740286; 1:50), CD19 (SJ25C1, BV711, BD Biosciences, catalog no. 563038; 5:100), CD27 (L128, BV785, BD Biosciences, catalog no. 563328; 2:50), CD38 [HIT2, allophycocyanin (APC)-Cy7, BioLegend, catalog no. 303534; 0.1:50], and immunoglobulin D (IgD) (IA6-2, PE-CF594, BioLegend, catalog no. 348240; 0.1:50). 4′,6-Diamidino-2-phenylindole was added before sample acquisition to allow dead cell exclusion. Gating of plasmablasts was performed as previously described (*49*). Healthy controls data were from Ferreira-Gomes *et al.* (*50*).

Cell culture

Passage-matched fibroblasts (passages 4 to 15) were cultured in Dulbecco's modified Eagle's medium (DMEM) complete medium [DMEM high glucose (4.5 g/liter) supplemented with 2 mM L-glutamine, 1% antibiotics/antimycotics, 5% non-essential amino acids (NEAA), and 10% fetal bovine serum (FBS)]. Epstein-Barr virus–transformed LCLs were cultured in RPMI 1640 complete medium (RPMI 1640 supplemented with 2 mM L-glutamine, 1% antibiotics/antimycotics, 5% NEAA, and 10% FBS). For isolation of human PBMCs, whole blood, diluted with phosphate-buffered saline (PBS), was gently layered over an equal volume of BioColl (Sigma-Aldrich) and centrifuged for 30 min at 400*g* without brake. The intermediate layer containing PBMCs was removed and added to prewarmed medium.

Retroviral transduction and fluorescence-activated cell sorting

For retroviral transduction of human citrine-tagged UNC93B1 into HEK293 cells, the pR 5′ LTR-hUNC93B plasmid was used. The E92G mutation was introduced by site-directed mutagenesis using the QuikChange Lightning Site-Directed Mutagenesis Kit (Agilent). For each viral supernatant to be produced, 1×10^6 HEK293T cells were plated in 2 ml of complete DMEM. After 24 hours, cells were transfected with retroviral constructs (1 μg per well), the retroviral packaging plasmids gag-pol (1 μg per well), and vesicular stomatitis virus glycoprotein (VSV-G) (1 μg per well) using polyethylenimine (Sigma-Aldrich). Cells were incubated at 37°C and 5% CO_2 for 12 hours, before medium change. Forty-eight hours upon transfection, the viral supernatant was harvested and added to target cells:

HEK293XL-hTLR3-HA, HEK293XL-hTLR7-HA, HEK293XL-hTLR8-HA, or HEK293XL-hTLR9-HA cells (Invivogen), seeded to 80% confluence. After 24 hours at 37°C and 5% CO_2, medium was changed to complete DMEM, and transduced cells were passaged three times before frozen stocks were prepared. UNC93B1-mCitrine–positive cells were sorted for equal green fluorescence on a FACSAria cell sorter (BD Biosciences) in a 96-well plate at a density of 2×10^4 cells per well in DMEM supplemented with 10% FBS, 2 mM L-glutamine, 1% antibiotics/antimycotics, and blasticidin (1 mg/ml).

HA (YPYDVPDYA)–tagged murine TLR3, TLR7, and TLR9 were expressed in *Unc93b1*$^{-/-}$ RAW264.7 cells using murine stem cell virus (MCSV)–Thy1.1 retroviral vectors as previously described (*37*). For the generation of *Unc93b1*-transgenic RAW264.7 cells, Unc_WT, Unc_H412R, and Unc_D34A constructs were generated as previously reported (*11*) on MCSV-based retroviral vectors with IRES-PuromycinR-T2A-mCherry double selection. *Unc93b1* genes were codon-optimized and contained a 3xFlag C-terminal tag. Unc_E92G construct was generated by site-directed mutagenesis from Unc_WT using Q5 Site Directed Mutagenesis Kit (New England Biolabs) and the following primers: forward, CACTACGACGgcACATACAGAGAAG; reverse, CAGGATCAGCTGCATCTG. Viral supernatants were produced by transfecting GP2-293 cells (HEK293-derived packaging cells expressing viral gag and pol proteins) with the Unc93b1 plasmids (1.7 μg per well) along with a VSV-G plasmid (0.8 μg per well) and preincubated with Lipofectamine 3000 transfection reagent (Invitrogen). After overnight incubation at 37°C, the transfected GP2-293 cells were transferred to 32°C for a further 24 hours. Viral supernatants were centrifuged to remove packaging cells before applying to *Unc93b1*$^{-/-}$ RAW264.7 target cells, with the addition of polybrene (Sigma-Aldrich). Target cells were centrifuged at 1000*g* for 30 min at 32°C and further incubated at 32°C overnight before transferring to a 37°C incubator (5% CO_2 maintained throughout). Unc93b1-IRES-mCherry–positive RAW264.7 cells were sorted 2 days after transduction for equal red fluorescence on a FACSAria II cell sorter (BD Biosciences) and cultured in RPMI 1640 supplemented with 10% FBS, L-glutamine, penicillin-streptomycin, sodium pyruvate, and Hepes (pH 7.2; Invitrogen). *Tlr7* expression in *Unc93b1*-reconstituted RAW264.7 cells was measured by fixation/permeabilization using BD Cytofix/Cytoperm (BD Biosciences), intracellular staining with anti-TLR7 antibody (Sigma-Aldrich, clone A94B10, MABF2273; 1:200), followed by Alexa Fluor 488 goat anti-mouse IgG (Invitrogen, A11029; 1:1000) and data acquisition on a FACSymphony flow cytometer (BD Biosciences).

Cytokine analysis

Plasma was collected from blood collected in heparin tubes by centrifugation (2000 rpm) at 4°C for 20 min. Cytokines were measured using the LEGENDplex Human Inflammation Panel 1 (BioLegend) according to the manufacturer's instructions. For experiments using PBMCs or stably transduced HEK293XL cells, cytokines were measured in cell culture supernatants using the LEGENDplex Human Anti-Virus Response Panel (BioLegend) according to the manufacturer's instructions. Data were collected on a FACS flow cytometer (LSRII, BD Biosciences) and analyzed with LEGENDplex Data Analysis V8.1 software (BioLegend). For cytokine analysis of whole blood assays, frozen supernatants were thawed on ice, and the cytokine concentration was quantified using the CorPlex Human Cytokine Panel 1 10-Plex Array (Quanterix) following the manufacturer's protocol. The samples were acquired on the Quanterix SP-X, and raw data were analyzed using SPX Analysis Application software version 2.1.1.7737. Cytokine concentration data were loaded into R version 4.2.2 (R Foundation for Statistical Computing) visualized using the tidyverse package version 1.3.2 (*51*). In RAW264.7 cells, TNF-α production was measured by fixation/permeabilization using BD Cytofix/Cytoperm (BD Biosciences) and intracellular staining with APC anti-mouse TNF-α antibody (BioLegend, clone MP6-XT22, 506308; 1:200), followed by acquisition on a CytoFLEX flow cytometer (Beckman Coulter). Flow cytometric data were analyzed using FlowJo (BD Biosciences).

Immunoprecipitation and Western blot analysis

For Myd88 immunoprecipitation, RAW264.7 cells were incubated with R848 (500 ng/ml) at 37°C and 5% CO_2 for 0, 15, 30, or 60 min before collection. Cells were collected by scraping in cold PBS; lysed in buffer containing 50 mM tris-HCl (pH 7.4), 150 mM NaCl, 10% glycerol, and 1% NP-40; and supplemented with cOmplete protease inhibitor cocktail (Roche), PhosSTOP (Roche), and 1 mM phenylmethylsulfonyl fluoride (PMSF). Cell lysates were incubated for 1 hour on a 4°C rotator, cleared of insoluble material by centrifugation, and then incubated with anti-MyD88 antibody (R&D Systems, AF3109; 1 μg per sample) overnight, followed by protein G agarose beads [preblocked with 1% bovine serum albumin (BSA)] for 2 hours at 4°C the next day. Beads were washed four times in lysis buffer, and then precipitated proteins were eluted by heating in SDS–polyacrylamide gel electrophoresis (PAGE) buffer to 65°C for 15 min.

For Flag immunoprecipitation, RAW264.7 cells were lysed in buffer containing 50 mM tris-HCl, 150 mM NaCl, 5 mM EDTA, 0.5% NP-40, 1× cOmplete protease inhibitor cocktail (Roche), and 1 mM PMSF. Cell lysates were incubated for 1 hour on a 4°C rotator, cleared of insoluble material by centrifugation, and then incubated with M2 anti-Flag matrix (Sigma-Aldrich) (preblocked with 1% BSA) for 2 hours on a 4°C rotator. Beads were washed four times in lysis buffer, and then precipitated proteins were competitively eluted with 3xFlag-peptide (150 ng/μl; Sigma-Aldrich) in lysis buffer for 30 min at room temperature. Eluted proteins were denatured in SDS-PAGE buffer for 1 hour at room temperature. Proteins were separated by SDS-PAGE (Bio-Rad TGX precast gels) and transferred to Immobilon polyvinylidene difluoride membranes (Millipore) in a Trans-Blot Turbo transfer system (Bio-Rad). Membranes were probed with antibodies against MyD88 (R&D Systems, AF3109; 1:200), IRAK2 [Cell Signaling Technology (CST), #4367; 1:1000], Flag (Sigma-Aldrich, clone M2, F1804; 1:1000), HA (Roche, 3F10), and glyceraldehyde-3-phosphate dehydrogenase (GAPDH) (Invitrogen, GA1R, MA5-15738; 1:2000). Blots were developed using the ChemiDoc MP system (Bio-Rad).

For green fluorescent protein (GFP) immunoprecipitation, HEK293 cells were lysed in NP-40 buffer [50 mM tris (pH 7.4), 150 mM NaCl, 0.5% NP-40, and 5 mM EDTA] supplemented with 40 mM *N*-ethylmaleimide (Sigma-Aldrich), 1× cOmplete protease inhibitor cocktail, and 1× PhosSTOP phosphatase inhibitors (Roche). After incubation at 4°C for 1 hour, lysates were cleared of insoluble material by centrifugation. For immunoprecipitations, lysates were incubated with ChromoTek GFP-Trap magnetic agarose (ProteinTech) for 2 hours at 4°C and washed twice in PBS containing 0.5% NP-40. Precipitated proteins were eluted and denatured in 2× SDS loading buffer at room temperature for 1 hour. LCLs were lysed in radioimmunoprecipitation assay buffer [50 mM tris-HCl (pH 7.4), 150 mM NaCl, 1 mM EDTA, 1% Triton X-100, 1 mM sodium orthovanadate, and 20 mM sodium fluoride] supplemented with 1× cOmplete protease inhibitor

cocktail, 1× PhosSTOP phosphatase inhibitors (Roche), and deoxyribonuclease I (DNase I) (QIAGEN). Protein concentration was determined using a bicinchoninic acid kit (Thermo Fisher Scientific). Lysates and GFP-immunoprecipitated proteins were resolved in a 4 to 12% NuPAGE bis-tris gel and blotted onto a nitrocellulose membrane (Sigma-Aldrich, BA83). Membranes were blocked in 5% dry milk and probed with the following antibodies diluted 1:1000 in 5% BSA: rabbit anti-TLR7 (CST, #5632), rabbit anti-syntenin (CST, #27964), rabbit anti-GFP (CST, #2956), and mouse anti–β-actin (Sigma-Aldrich, #A5316). Immunoreactive signals were detected by chemiluminescence using Lumi-Light PLUS (Roche).

Cell stimulation

Cells were stimulated as indicated with poly(I:C) high molecular weight (HMW) (Invivogen, tlrl-pic), R848 (resiquimod, Invivogen, tlrl-r848), Pam2CSK4 (Invivogen, tlrl-pm2s-1), ODN2006 (Invivogen, tlrl-2006), ODN1668 (5′-TCCATGACGTTCCTGATGCT-3′, all phosphorothioate linkages, synthesized by Integrated DNA Technologies), LPS-EB Ultrapure (Invivogen, tlrl-3pelps), polyU_19mer (all phosphorothioate linkages, Integrated DNA Technologies), and ssRNA40 (5′-GCCCGUCUGUUGUGUGACUC-3′, Eurofins MWG Operon). If not otherwise indicated, then ssRNA40 and ODN2006 were complexed in a 1:1 ratio with poly-L-arginine (Sigma-Aldrich). Unless otherwise specified, cells were stimulated for 24 hours at 37°C and 5% CO_2. RAW264.7 macrophages were stimulated for 6 hours at 37°C and 5% CO_2, with the addition of BD GolgiPlug at 1:1000 dilution after 30 min of stimulation.

Whole-blood assay

For analysis of the effect of ruxolitinib on type I IFN signaling in vitro, heparin blood was distributed in 24-well plates at 1 ml per well. Plates were incubated on a shaker incubator at 300 rpm and 37°C. For type I IFN activation, blood was incubated with poly(I:C) HMW (1 μg/ml; Invivogen) for 5 hours and then either treated with 1 and 2 μM ruxolitinib (MedChemExpress) or left untreated for additional 10 hours. After erythrocyte lysis, samples were frozen at −80°C and subsequently used for RNA extraction. For analysis of induced cytokine responses in family A, hirudin blood was diluted with cell culture medium in a ratio of 1:3, activated with R848 (100 ng/ml; InvivoGen) or ADU-S100 (10 μg/ml; MedChemExpress) for 6 hours at 37°C, and centrifuged at 230*g* for 5 min at room temperature. For analysis of specific TLR responses, whole blood was diluted 1:1 with RPMI 1640 cell culture medium and stimulated for 24 hours with R837 (5 μg/ml; InvivoGen), TL8-506 (100 ng/ml; InvivoGen), or 1 μM ODN2216 (InvivoGen).

Quantitative real-time reverse transcription PCR

Total RNA was extracted from PBMCs or from lysed whole blood using the ReliaPrep RNA Cell Miniprep System (Promega), followed by DNase I digestion. RNA was reverse-transcribed using the GoScript Reverse Transcription System (Promega). Gene expression was determined by quantitative real-time reverse transcription (RT)–PCR using the TaqMan Universal PCR Master Mix (Applied Biosystems) on an ABI7300 and normalized to GAPDH [forward, GAAG GTGAAGGTCGGAGTC; reverse, GAAGATGGTGATGGGATT TC; and fluorescein amidite (FAM), CAAGCTTCCCGTTCTCA GCC-TAMRA] and hypoxanthine phosphoribosyltransferase 1 (Hs02800695_m1, Thermo Fisher Scientific) expression. For calibration, a calibrator cDNA was included in each assay. Target genes were analyzed using predesigned TaqMan probes (Thermo Fisher Scientific) for *IFI27* (Hs01086373_g1), *IFI44* (Hs00951349_m1), *IFI44L* (Hs00915292_m1), *IFIT1* (Hs01675197_m1), *ISG15* (Hs01921425_s1), *RSAD2* (Hs01057264_m1), and *SIGLEC1* (Hs00988063_m1). The IFN score was calculated as previously described (*42*).

Protein structure modeling

Illustration of the complex TLR7-UNC93B1 [Protein Data Bank (PDB): 7CYN] was prepared using UCSF ChimeraX (*52*).

Statistical analysis

Statistical analysis was carried out in GraphPad Prism 6 as indicated. For normally distributed variables, parametric tests were used, including *t* test for comparison of two groups and one-way analysis of variance (ANOVA) with post hoc tests, as indicated, for comparison of three or more groups. For variables with non-normal distribution, nonparametric tests were used. For comparison of two groups, Mann-Whitney *U* test was used for independent variables, and Wilcoxon signed-rank test was used for dependent variables. For comparison of three or more group variables, Kruskal-Wallis test was used. Values of $P < 0.05$ were considered statistically significant. Data are represented as means ± SD.

Supplementary Materials

This PDF file includes:

Figs. S1 to S11
Tables S1 to S4
References (*53*–*61*)

Other Supplementary Material for this manuscript includes the following:

Data S1 and S2
MDAR Reproducibility Checklist

REFERENCES AND NOTES

1. N. A. Lind, V. E. Rael, K. Pestal, B. Liu, G. M. Barton, Regulation of the nucleic acid-sensing Toll-like receptors. *Nat. Rev. Immunol.* **22**, 224–235 (2022).
2. K. Pelka, T. Shibata, K. Miyake, E. Latz, Nucleic acid-sensing TLRs and autoimmunity: Novel insights from structural and cell biology. *Immunol. Rev.* **269**, 60–75 (2016).
3. I. Botos, D. M. Segal, D. R. Davies, The structural biology of Toll-like receptors. *Structure* **19**, 447–459 (2011).
4. Y.-M. Kim, M. M. Brinkmann, M.-E. Paquet, H. L. Ploegh, UNC93B1 delivers nucleotide-sensing Toll-like receptors to endolysosomes. *Nature* **452**, 234–238 (2008).
5. M. M. Brinkmann, E. Spooner, K. Hoebe, B. Beutler, H. L. Ploegh, Y.-M. Kim, The interaction between the ER membrane protein UNC93B and TLR3, 7, and 9 is crucial for TLR signaling. *J. Cell Biol.* **177**, 265–275 (2007).
6. K. Pelka, D. Bertheloot, E. Reimer, K. Phulphagar, S. V. Schmidt, A. Christ, R. Stahl, N. Watson, K. Miyake, N. Hacohen, A. Haas, M. M. Brinkmann, A. Marshak-Rothstein, F. Meissner, E. Latz, The chaperone UNC93B1 regulates Toll-like receptor stability independently of endosomal TLR transport. *Immunity* **48**, 911–922.e7 (2018).
7. H. Ishida, J. Asami, Z. Zhang, T. Nishizawa, H. Shigematsu, U. Ohto, T. Shimizu, Cryo-EM structures of Toll-like receptors in complex with UNC93B1. *Nat. Struct. Mol. Biol.* **28**, 173–180 (2021).
8. K. Tabeta, K. Hoebe, E. M. Janssen, X. Du, P. Georgel, K. Crozat, S. Mudd, N. Mann, S. Sovath, J. Goode, L. Shamel, A. A. Herskovits, D. A. Portnoy, M. Cooke, L. M. Tarantino, T. Wiltshire, B. E. Steinberg, S. Grinstein, B. Beutler, The Unc93b1 mutation 3d disrupts exogenous antigen presentation and signaling via Toll-like receptors 3, 7 and 9. *Nat. Immunol.* **7**, 156–164 (2006).
9. A. Casrouge, S.-Y. Zhang, C. Eidenschenk, E. Jouanguy, A. Puel, K. Yang, A. Alcais, C. Picard, N. Mahfoufi, N. Nicolas, L. Lorenzo, S. Plancoulaine, B. Sénéchal, F. Geissmann, K. Tabeta, K. Hoebe, X. Du, R. L. Miller, B. Héron, C. Mignot, T. B. de Villemeur, P. Lebon, O. Dulac, F. Rozenberg, B. Beutler, M. Tardieu, L. Abel, J.-L. Casanova, Herpes simplex virus encephalitis in human UNC-93B deficiency. *Science* **314**, 308–312 (2006).
10. J.-W. Huh, T. Shibata, M. Hwang, E.-H. Kwon, M. S. Jang, R. Fukui, A. Kanno, D.-J. Jung, M. H. Jang, K. Miyake, Y.-M. Kim, UNC93B1 is essential for the plasma membrane

localization and signaling of Toll-like receptor 5. *Proc. Natl. Acad. Sci. U.S.A.* **111**, 7072–7077 (2014).
11. O. Majer, B. Liu, L. S. M. Kreuk, N. Krogan, G. M. Barton, UNC93B1 recruits syntenin-1 to dampen TLR7 signalling and prevent autoimmunity. *Nature* **575**, 366–370 (2019).
12. S. R. Christensen, J. Shupe, K. Nickerson, M. Kashgarian, R. A. Flavell, M. J. Shlomchik, Toll-like receptor 7 and TLR9 dictate autoantibody specificity and have opposing inflammatory and regulatory roles in a murine model of lupus. *Immunity* **25**, 417–428 (2006).
13. P. Pisitkun, J. A. Deane, M. J. Difilippantonio, T. Tarasenko, A. B. Satterthwaite, S. Bolland, Autoreactive B cell responses to RNA-related antigens due to TLR7 gene duplication. *Science* **312**, 1669–1672 (2006).
14. S. Subramanian, K. Tus, Q.-Z. Li, A. Wang, X.-H. Tian, J. Zhou, C. Liang, G. Bartov, L. D. McDaniel, X. J. Zhou, R. A. Schultz, E. K. Wakeland, A Tlr7 translocation accelerates systemic autoimmunity in murine lupus. *Proc. Natl. Acad. Sci. U.S.A.* **103**, 9970–9975 (2006).
15. R. Fukui, S.-I. Saitoh, A. Kanno, M. Onji, T. Shibata, A. Ito, M. Onji, M. Matsumoto, S. Akira, N. Yoshida, K. Miyake, Unc93B1 restricts systemic lethal inflammation by orchestrating Toll-like receptor 7 and 9 trafficking. *Immunity* **35**, 69–81 (2011).
16. S. A. Jenks, K. S. Cashman, E. Zumaquero, U. M. Marigorta, A. V. Patel, X. Wang, D. Tomar, M. C. Woodruff, Z. Simon, R. Bugrovsky, E. L. Blalock, C. D. Scharer, C. M. Tipton, C. Wei, S. S. Lim, M. Petri, T. B. Niewold, J. H. Anolik, G. Gibson, F. E.-H. Lee, J. M. Boss, F. E. Lund, I. Sanz, Distinct effector b cells induced by unregulated Toll-like receptor 7 contribute to pathogenic responses in systemic lupus erythematosus. *Immunity* **49**, 725–739.e6 (2018).
17. G. J. Brown, P. F. Cañete, H. Wang, A. Medhavy, J. Bones, J. A. Roco, Y. He, Y. Qin, J. Cappello, J. I. Ellyard, K. Bassett, Q. Shen, G. Burgio, Y. Zhang, C. Turnbull, X. Meng, P. Wu, E. Cho, L. A. Miosge, T. D. Andrews, M. A. Field, D. Tvorogov, A. F. Lopez, J. J. Babon, C. A. López, Á. Gónzalez-Murillo, D. C. Garulo, V. Pascual, T. Levy, E. J. Mallack, D. G. Calame, T. Lotze, J. R. Lupski, H. Ding, T. R. Ullah, G. D. Walters, M. E. Koina, M. C. Cook, N. Shen, C. de Lucas Collantes, B. Corry, M. P. Gantier, V. Athanasopoulos, C. G. Vinuesa, TLR7 gain-of-function genetic variation causes human lupus. *Nature* **605**, 349–356 (2022).
18. Z. Zhang, U. Ohto, T. Shibata, E. Krayukhina, M. Taoka, Y. Yamauchi, H. Tanji, T. Isobe, S. Uchiyama, K. Miyake, T. Shimizu, Structural analysis reveals that Toll-like receptor 7 is a dual receptor for guanosine and single-stranded RNA. *Immunity* **45**, 737–748 (2016).
19. D. Nehar-Belaid, S. Hong, R. Marches, G. Chen, M. Bolisetty, J. Baisch, L. Walters, M. Punaro, R. J. Rossi, C.-H. Chung, R. P. Huynh, P. Singh, W. F. Flynn, J.-A. Tabanor-Gayle, N. Kuchipudi, A. Mejias, M. A. Collet, A. L. Lucido, K. Palucka, P. Robson, S. Lakshminarayanan, O. Ramilo, T. Wright, V. Pascual, J. F. Banchereau, Mapping systemic lupus erythematosus heterogeneity at the single-cell level. *Nat. Immunol.* **21**, 1094–1106 (2020).
20. C. Guiducci, M. Gong, Z. Xu, M. Gill, D. Chaussabel, T. Meeker, J. H. Chan, T. Wright, M. Punaro, S. Bolland, V. Soumelis, J. Banchereau, R. L. Coffman, V. Pascual, F. J. Barrat, TLR recognition of self nucleic acids hampers glucocorticoid activity in lupus. *Nature* **465**, 937–941 (2010).
21. R. K. Perez, M. G. Gordon, M. Subramaniam, M. C. Kim, G. C. Hartoularos, S. Targ, Y. Sun, A. Ogorodnikov, R. Bueno, A. Lu, M. Thompson, N. Rappoport, A. Dahl, C. M. Lanata, M. Matloubian, L. Maliskova, S. S. Kwek, T. Li, M. Slyper, J. Waldman, D. Dionne, O. Rozenblatt-Rosen, L. Fong, M. Dall'Era, B. Balliu, A. Regev, J. Yazdany, L. A. Criswell, N. Zaitlen, C. J. Ye, Single-cell RNA-seq reveals cell type-specific molecular and genetic associations to lupus. *Science* **376**, eabf1970 (2022).
22. A. M. Jacobi, M. Odendahl, K. Reiter, A. Bruns, G. R. Burmester, A. Radbruch, G. Valet, P. E. Lipsky, T. Dörner, Correlation between circulating CD27highplasma cells and disease activity in patients with systemic lupus erythematosus. *Arthritis Rheum.* **48**, 1332–1342 (2003).
23. F. Heil, H. Hemmi, H. Hochrein, F. Ampenberger, C. Kirschning, S. Akira, G. Lipford, H. Wagner, S. Bauer, Species-specific recognition of single-stranded RNA via Toll-like receptor 7 and 8. *Science* **303**, 1526–1529 (2004).
24. A. Kuznik, M. Bencina, U. Svajger, M. Jeras, B. Rozman, R. Jerala, Mechanism of endosomal TLR inhibition by antimalarial drugs and imidazoquinolines. *J. Immunol.* **186**, 4794–4804 (2011).
25. I. B. Bekeredjian-Ding, M. Wagner, V. Hornung, T. Giese, M. Schnurr, S. Endres, G. Hartmann, Plasmacytoid dendritic cells control TLR7 sensitivity of naive B cells via type I IFN. *J. Immunol.* **174**, 4043–4050 (2005).
26. A. Marshak-Rothstein, Toll-like receptors in systemic autoimmune disease. *Nat. Rev. Immunol.* **6**, 823–835 (2006).
27. F. P. Siegal, N. Kadowaki, M. Shodell, P. A. Fitzgerald-Bocarsly, K. Shah, S. Ho, S. Antonenko, Y. J. Liu, The nature of the principal type 1 interferon-producing cells in human blood. *Science* **284**, 1835–1837 (1999).
28. W. Greulich, M. Wagner, M. M. Gaidt, C. Stafford, Y. Cheng, A. Linder, T. Carell, V. Hornung, TLR8 is a sensor of RNase T2 degradation products. *Cell* **179**, 1264–1275.e13 (2019).
29. R. Fukui, S. Saitoh, F. Matsumoto, H. Kozuka-Hata, M. Oyama, K. Tabeta, B. Beutler, K. Miyake, Unc93B1 biases Toll-like receptor responses to nucleic acid in dendritic cells toward DNA- but against RNA-sensing. *J. Exp. Med.* **206**, 1339–1350 (2009).
30. S. Sharma, A. M. Campbell, J. Chan, S. A. Schattgen, G. M. Orlowski, R. Nayar, A. H. Huyler, K. Nündel, C. Mohan, L. J. Berg, M. J. Shlomchik, A. Marshak-Rothstein, K. A. Fitzgerald, Suppression of systemic autoimmunity by the innate immune adaptor STING. *Proc. Natl. Acad. Sci. U.S.A.* **112**, E710–E717 (2015).
31. J. Aluri, A. Bach, S. Kaviany, L. Chiquetto Paracatu, M. Kitcharoensakkul, M. A. Walkiewicz, C. D. Putnam, M. Shinawi, N. Saucier, E. M. Rizzi, M. T. Harmon, M. P. Keppel, M. Ritter, M. Similuk, E. Kulm, M. Joyce, A. A. de Jesus, R. Goldbach-Mansky, Y.-S. Lee, M. Cella, P. L. Kendall, M. C. Dinauer, J. J. Bednarski, C. Bemrich-Stolz, S. W. Canna, S. M. Abraham, M. M. Demczko, J. Powell, S. M. Jones, A. M. Scurlock, S. S. De Ravin, J. J. Bleesing, J. A. Connelly, V. K. Rao, L. G. Schuettpelz, M. A. Cooper, Immunodeficiency and bone marrow failure with mosaic and germline TLR8 gain of function. *Blood* **137**, 2450–2462 (2021).
32. V. Hornung, S. Rothenfusser, S. Britsch, A. Krug, B. Jahrsdörfer, T. Giese, S. Endres, G. Hartmann, Quantitative expression of Toll-like receptor 1-10 mRNA in cellular subsets of human peripheral blood mononuclear cells and sensitivity to CpG oligodeoxynucleotides. *J. Immunol.* **168**, 4531–4537 (2002).
33. Z. Zhang, U. Ohto, T. Shibata, M. Taoka, Y. Yamauchi, R. Sato, N. M. Shukla, S. A. David, T. Isobe, K. Miyake, T. Shimizu, Structural analyses of Toll-like receptor 7 reveal detailed RNA sequence specificity and recognition mechanism of agonistic ligands. *Cell Rep.* **25**, 3371–3381.e5 (2018).
34. T. Shibata, U. Ohto, S. Nomura, K. Kibata, Y. Motoi, Y. Zhang, Y. Murakami, R. Fukui, T. Ishimoto, S. Sano, T. Ito, T. Shimizu, K. Miyake, Guanosine and its modified derivatives are endogenous ligands for TLR7. *Int. Immunol.* **28**, 211–222 (2016).
35. H. Tanji, U. Ohto, T. Shibata, M. Taoka, Y. Yamauchi, T. Isobe, K. Miyake, T. Shimizu, Toll-like receptor 8 senses degradation products of single-stranded RNA. *Nat. Struct. Mol. Biol.* **22**, 109–115 (2015).
36. T. Ostendorf, T. Zillinger, K. Andryka, T. M. Schlee-Guimaraes, S. Schmitz, S. Marx, K. Bayrak, R. Linke, S. Salgert, J. Wegner, T. Grasser, S. Bauersachs, L. Soltesz, M. P. Hübner, M. Nastaly, C. Coch, M. Kettwig, I. Roehl, M. Henneke, A. Hoerauf, W. Barchet, J. Gärtner, M. Schlee, G. Hartmann, E. Bartok, Immune sensing of synthetic, bacterial, and protozoan RNA by Toll-like receptor 8 requires coordinated processing by RNase T2 and RNase 2. *Immunity* **52**, 591–605.e6 (2020).
37. O. Majer, B. Liu, B. J. Woo, L. S. M. Kreuk, E. Van Dis, G. M. Barton, Release from UNC93B1 reinforces the compartmentalized activation of select TLRs. *Nature* **575**, 371–374 (2019).
38. H. Mishra, C. Schlack-Leigers, E. L. Lim, O. Thieck, T. Magg, J. Raedler, C. Wolf, C. Klein, H. Ewers, M. A. Lee-Kirsch, D. Meierhofer, F. Hauck, O. Majer, Disrupted degradative sorting of TLR7 is associated with human lupus. *Sci. Immunol.* **9**, eadi9575 (2024).
39. S. Hawtin, C. André, G. Collignon-Zipfel, S. Appenzeller, B. Bannert, L. Baumgartner, D. Beck, C. Betschart, T. Boulay, H. I. Brunner, M. Ceci, J. Deane, R. Feifel, E. Ferrero, D. Kyburz, F. Lafossas, P. Loetscher, C. Merz-Stoeckle, P. Michellys, B. Nuesslein-Hildesheim, F. Raulf, J. S. Rush, G. Ruzzante, T. Stein, S. Zaharevitz, G. Wieczorek, R. Siegel, P. Gergely, T. Shisha, T. Junt, Preclinical characterization of the Toll-like receptor 7/8 antagonist MHV370 for lupus therapy. *Cell. Rep. Med.* **4**, 101036 (2023).
40. T. Shisha, M. G. Posch, J. Lehmann, R. Feifel, T. Junt, S. Hawtin, J. Schuemann, A. Avrameas, R. Danekula, P. Misiolek, R. Siegel, P. Gergely, First-in-human study of the safety, pharmacokinetics, and pharmacodynamics of MHV370, a dual inhibitor of Toll-like receptors 7 and 8, in healthy adults. *Eur. J. Drug Metab. Pharmacokinet.* **48**, 553–566 (2023).
41. T. Leeb, F. Leuthard, V. Jagannathan, S. Kiener, A. Letko, P. Roosje, M. M. Welle, K. L. Gailbreath, A. Cannon, M. Linek, F. Banovic, T. Olivry, S. D. White, K. Batcher, D. Bannasch, K. M. Minor, J. R. Mickelson, M. K. Hytönen, H. Lohi, E. A. Mauldin, M. L. Casal, A missense variant affecting the C-terminal tail of UNC93B1 in dogs with exfoliative cutaneous lupus erythematosus (ECLE). *Genes (Basel)* **11**, 159 (2020).
42. C. Wolf, N. Brück, S. Koss, C. Griep, M. Kirschfink, K. Palm-Beden, M. Fang, N. Röber, S. Winkler, R. Berner, E. Latz, C. Günther, M. A. Lee-Kirsch, Janus kinase inhibition in complement component 1 deficiency. *J. Allergy Clin. Immunol.* **146**, 1439–1442.e5 (2020).
43. Y. Chen, Y. Chen, C. Shi, Z. Huang, Y. Zhang, S. Li, Y. Li, J. Ye, C. Yu, Z. Li, X. Zhang, J. Wang, H. Yang, L. Fang, Q. Chen, SOAPnuke: A MapReduce acceleration-supported software for integrated quality control and preprocessing of high-throughput sequencing data. *Gigascience* **7**, 1–6 (2018).
44. H. Li, R. Durbin, Fast and accurate long-read alignment with Burrows-Wheeler transform. *Bioinformatics* **26**, 589–595 (2010).
45. A. McKenna, M. Hanna, E. Banks, A. Sivachenko, K. Cibulskis, A. Kernytsky, K. Garimella, D. Altshuler, S. Gabriel, M. Daly, M. A. DePristo, The genome analysis toolkit: A MapReduce framework for analyzing next-generation DNA sequencing data. *Genome Res.* **20**, 1297–1303 (2010).
46. W. McLaren, L. Gil, S. E. Hunt, H. S. Riat, G. R. S. Ritchie, A. Thormann, P. Flicek, F. Cunningham, The Ensembl variant effect predictor. *Genome Biol.* **17**, 122 (2016).
47. M. Holtgrewe, O. Stolpe, M. Nieminen, S. Mundlos, A. Knaus, U. Kornak, D. Seelow, L. Segebrecht, M. Spielmann, B. Fischer-Zirnsak, F. Boschann, U. Scholl, N. Ehmke, D. Beule, VarFish: Comprehensive DNA variant analysis for diagnostics and research. *Nucleic Acids Res.* **48**, W162–W169 (2020).
48. D. Hombach, M. Schuelke, E. Knierim, N. Ehmke, J. M. Schwarz, B. Fischer-Zirnsak, D. Seelow, MutationDistiller: User-driven identification of pathogenic DNA variants. *Nucleic Acids Res.* **47**, W114–W120 (2019).

49. F. Szelinski, A. L. Stefanski, E. Schrezenmeier, H. Rincon-Arevalo, A. Wiedemann, K. Reiter, J. Ritter, M. Lettau, V. D. Dang, S. Fuchs, A. P. Frei, T. Alexander, A. C. Lino, T. Dörner, Plasmablast-like phenotype among antigen-experienced CXCR5−CD19^{low} B cells in systemic lupus erythematosus. *Arthritis Rheumatol.* **74**, 1556–1568 (2022).
50. M. Ferreira-Gomes, A. Kruglov, P. Durek, F. Heinrich, C. Tizian, G. A. Heinz, A. Pascual-Reguant, W. Du, R. Mothes, C. Fan, S. Frischbutter, K. Habenicht, L. Budzinski, J. Ninnemann, P. K. Jani, G. M. Guerra, K. Lehmann, M. Matz, L. Ostendorf, L. Heiberger, H.-D. Chang, S. Bauherr, M. Maurer, G. Schönrich, M. Raftery, T. Kallinich, M. A. Mall, S. Angermair, S. Treskatsch, T. Dörner, V. M. Corman, A. Diefenbach, H.-D. Volk, S. Elezkurtaj, T. H. Winkler, J. Dong, A. E. Hauser, H. Radbruch, M. Witkowski, F. Melchers, A. Radbruch, M.-F. Mashreghi, SARS-CoV-2 in severe COVID-19 induces a TGF-β-dominated chronic immune response that does not target itself. *Nat. Commun.* **12**, 1961 (2021).
51. H. Wickham, M. Averick, J. Bryan, W. Chang, L. D. McGowan, R. François, G. Grolemund, A. Hayes, L. Henry, J. Hester, M. Kuhn, T. L. Pedersen, E. Miller, S. M. Bache, K. Müller, J. Ooms, D. Robinson, D. P. Seidel, V. Spinu, K. Takahashi, D. Vaughan, C. Wilke, K. Woo, H. Yutani, Welcome to the Tidyverse. *J. Open Source Softw.* **4**, 1686 (2019).
52. T. D. Goddard, C. C. Huang, E. C. Meng, E. F. Pettersen, G. S. Couch, J. H. Morris, T. E. Ferrin, UCSF ChimeraX: Meeting modern challenges in visualization and analysis. *Protein Sci.* **27**, 14–25 (2018).
53. M. Witkowski, C. Tizian, M. Ferreira-Gomes, D. Niemeyer, T. C. Jones, F. Heinrich, S. Frischbutter, S. Angermair, T. Hohnstein, I. Mattiola, P. Nawrath, S. McEwen, S. Zocche, E. Viviano, G. A. Heinz, M. Maurer, U. Kölsch, R. L. Chua, T. Aschman, C. Meisel, J. Radke, B. Sawitzki, J. Roehmel, K. Allers, V. Moos, T. Schneider, L. Hanitsch, M. A. Mall, C. Conrad, H. Radbruch, C. U. Duerr, J. A. Trapani, E. Marcenaro, T. Kallinich, V. M. Corman, F. Kurth, L. E. Sander, C. Drosten, S. Treskatsch, P. Durek, A. Kruglov, A. Radbruch, M.-F. Mashreghi, A. Diefenbach, Untimely TGFβ responses in COVID-19 limit antiviral functions of NK cells. *Nature* **600**, 295–301 (2021).
54. Y. Huang, D. J. McCarthy, O. Stegle, Vireo: Bayesian demultiplexing of pooled single-cell RNA-seq data without genotype reference. *Genome Biol.* **20**, 273 (2019).
55. C. S. McGinnis, L. M. Murrow, Z. J. Gartner, DoubletFinder: Doublet detection in single-cell RNA sequencing data using artificial nearest neighbors. *Cell Syst.* **8**, 329–337.e4 (2019).
56. F. A. Wolf, P. Angerer, F. J. Theis, SCANPY: Large-scale single-cell gene expression data analysis. *Genome Biol.* **19**, 15 (2018).
57. Y. Xu, S. J. Baumgart, C. M. Stegmann, S. Hayat, MACA: Marker-based automatic cell-type annotation for single-cell expression data. *Bioinformatics* **38**, 1756–1760 (2022).
58. Y. Hao, S. Hao, E. Andersen-Nissen, W. M. Mauck, S. Zheng, A. Butler, M. J. Lee, A. J. Wilk, C. Darby, M. Zager, P. Hoffman, M. Stoeckius, E. Papalexi, E. P. Mimitou, J. Jain, A. Srivastava, T. Stuart, L. M. Fleming, B. Yeung, A. J. Rogers, J. M. McElrath, C. A. Blish, R. Gottardo, P. Smibert, R. Satija, Integrated analysis of multimodal single-cell data. *Cell* **184**, 3573–3587.e29 (2021).
59. E. Y. Chen, C. M. Tan, Y. Kou, Q. Duan, Z. Wang, G. V. Meirelles, N. R. Clark, A. Ma'ayan, Enrichr: Interactive and collaborative HTML5 gene list enrichment analysis tool. *BMC Bioinformatics* **14**, 128 (2013).
60. A. Butler, P. Hoffman, P. Smibert, E. Papalexi, R. Satija, Integrating single-cell transcriptomic data across different conditions, technologies, and species. *Nat. Biotechnol.* **36**, 411–420 (2018).
61. M. Aringer, K. Costenbader, D. Daikh, R. Brinks, M. Mosca, R. Ramsey-Goldman, J. S. Smolen, D. Wofsy, D. T. Boumpas, D. L. Kamen, D. Jayne, R. Cervera, N. Costedoat-Chalumeau, B. Diamond, D. D. Gladman, B. Hahn, F. Hiepe, S. Jacobsen, D. Khanna, K. Lerstrøm, E. Massarotti, J. McCune, G. Ruiz-Irastorza, J. Sanchez-Guerrero, M. Schneider, M. Urowitz, G. Bertsias, B. F. Hoyer, N. Leuchten, C. Tani, S. K. Tedeschi, Z. Touma, G. Schmajuk, B. Anic, F. Assan, T. M. Chan, A. E. Clarke, M. K. Crow, L. Czirják, A. Doria, W. Graninger, B. Halda-Kiss, S. Hasni, P. M. Izmirly, M. Jung, G. Kumánovics, X. Mariette, I. Padjen, J. M. Pego-Reigosa, J. Romero-Diaz, Í. Rúa-Figueroa Fernández, R. Seror, G. H. Stummvoll, Y. Tanaka, M. G. Tektonidou, C. Vasconcelos, E. M. Vital, D. J. Wallace, S. Yavuz, P. L. Meroni, M. J. Fritzler, R. Naden, T. Dörner, S. R. Johnson, 2019 European League Against Rheumatism/American College of Rheumatology classification criteria for systemic lupus erythematosus. *Ann. Rheum. Dis.* **78**, 1151–1159 (2019).

Acknowledgments: We thank the patients and their family for participation in the study. We thank A. Gompf, R. Stahl, and M. Utzt for technical assistance; S.-Y. Zhang and J.-L. Casanova for UNC93B1-deficient patient cells; and T. Straub and the Bioinformatic Core Facility for providing compute infrastructure. We acknowledge the assistance of the flow cytometry and the imaging facilities of the Center for Molecular and Cellular Bioengineering and the Medical Theoretical Centre, TU Dresden, the flow cytometry and sequencing facilities of the Deutsches Rheuma-Forschungszentrum, Berlin, as well as the LAFUGA sequencing facility of the Gene Center LMU, Munich. **Funding:** The study was supported by German Research Foundation (DFG) grants KFO249 160548243 (to M.A.L.-K.), CRC237 369799452/B21 (to M.A.L.-K. and J.K.), CRC237 369799452/A11 (to M.A.L.-K. and E.L.), CRC237 369799452/A06 (to C.W.), KI 1956/2-1 (to B.K.), the Emmy Noether Program 458004906 (to C.C.d.O.M.), the German Federal Ministry of Education and Research grants 01GM2206C (to M.A.L.-K.), CONAN and TReAT (to M.-F.M.), an Else-Kröner-Fresenius-Stiftung starting grant 2019_A70 (to J.K.), the Leibniz Association, Leibniz Collaborative Excellence, TargArt (to T.K. and M.-F.M.) and ImpACt (to M.-F.M.), the Berlin Institute of Health with the state of Berlin and the European Regional Development Fund (ERDF 2014–2021, EFRE 1.8/11, Deutsches Rheuma-Forschungszentrum) (to M.-F.M.), a Berlin Institute of Health Fellowship (to T.K.), a Berlin Institute of Health Clinical Scientist Program Fellowship (to C.C.G.), and the Max Planck Society (to E.L.L. and O.M.). **Author contributions:** Conceptualization: C.W. and M.A.L.-K. Methodology: C.W., E.L.L., M. Mokhtari, P.D., A.S., E.B., M.-F.M., S.V.S., J.K., O.M., and M.A.L.-K. Investigation: C.W., E.L.L., M. Mokhtari, B.K., A.O., E.L.-V., S.K., S.M., K. Menzel, K.E., G.D., B.B., D.T.S., K.S., T.N., C.C.G., P.D., K. Minden, T.D., A.S., F.S., G.M.G., M. Massoud, M.B., C.C.d.O.M., E.B., T.K., M.-F.M., S.V.S., E.L., J.K., O.M., and M.A.L.-K. Visualization: C.W., E.L., M. Mokhtari, C.C.d.O.M., J.K., and O.M. Funding acquisition: C.W., E.L.L., B.K., E.L., C.C.d.O.M., M.-F.M., T.K., C.C.G., J.K., O.M., and M.A.L.-K. Project administration: M.A.L.-K. Supervision: C.W., J.K., O.M., and M.A.L.-K. Writing (original draft): C.W. and M.A.L.-K. Writing (review and editing): C.W., J.K., O.M., and M.A.L.-K. **Competing interests:** E.L. is cofounder and advisor of IFM Therapeutics, Odyssey Therapeutics, and Beren Therapeutics. All other authors declare that they have no competing interests. **Data and materials availability:** scRNA sequencing data reported in this study have been deposited in the single-cell portal for interactive viewing and download (accession number SCP2151) and GEO (accession number GSE250223). Jupyter notebooks and scripts used for the analysis of scRNA sequencing data are available on GitHub (https://github.com/KlughammerLab/UNC93B1_scRNAseq) and Zenodo (https://zenodo.org/doi/10.5281/zenodo.10395384). Tabulated data underlying the figures are provided in data file S1 and uncropped Western blots in data file S2. All other data needed to support the conclusions of the paper are available in the main text or the Supplementary Materials.

Submitted 30 May 2023
Accepted 22 December 2023
Published First Release 11 January 2024
Final published 23 February 2024
10.1126/sciimmunol.adi9769